JCI insight

# Neonatal hyperoxia inhibits proliferation and survival of atrial cardiomyocytes by suppressing fatty acid synthesis

Ethan David Cohen, … , Gloria S. Pryhuber, Michael A. O'Reilly

*JCI Insight.* 2021. https://doi.org/10.1172/jci.insight.140785.

**Research** In-Press Preview **Cardiology**

Preterm birth increases the risk for pulmonary hypertension and heart failure in adulthood. Oxygen therapy can damage the immature cardiopulmonary system and may be partially responsible for the cardiovascular disease in adults born preterm. We previously showed that exposing newborn mice to hyperoxia causes pulmonary hypertension by 1 year of age that is preceded by a poorly understood loss of pulmonary vein cardiomyocyte proliferation. We now show that hyperoxia also reduces cardiomyocyte proliferation and survival in the left atrium and causes diastolic heart failure by disrupting its filling of the left ventricle. Transcriptomic profiling showed that neonatal hyperoxia permanently suppressed fatty acid synthase (*Fasn*), stearoyl-CoA desaturase 1 (*Scd1*) and other fatty acid synthesis genes in the atria of mice, the HL-1 line of mouse atrial cardiomyocytes and left atrial tissue explanted from human infants. Suppressing *Fasn* or *Scd1* reduced HL-1 cell proliferation and increased cell death while overexpressing these genes maintained their expansion in hyperoxia, suggesting oxygen directly inhibits atrial cardiomyocyte proliferation and survival by repressing *Fasn* and *Scd1*. Pharmacologic interventions that restore *Fasn*, *Scd1* and other fatty acid synthesis genes in atrial cardiomyocytes may thus provide a way of ameliorating the adverse effects of supplemental oxygen on preterm infants.



# Neonatal hyperoxia inhibits proliferation and survival of atrial cardiomyocytes by suppressing fatty acid synthesis

Ethan David Cohen[1,4]
Min Yee[1]
George A. Porter, Jr.[1]
Erin Ritzer[1]
Andrew N. McDavid[2]
Paul S. Brookes[3]
Gloria S. Pryhuber[1]
Michael A. O'Reilly[1,4]

The Departments of [1]Pediatrics, [2]Biostatistics & Computational Biology, and [3]Anesthesiology
School of Medicine and Dentistry, The University of Rochester, Rochester NY 14642

[4]**Address Correspondence to**:

Ethan David Cohen, Ph.D.
Department of Pediatrics
Box 850
The University of Rochester
School of Medicine and Dentistry
601 Elmwood Avenue
Rochester, NY 14642
Tel: (585) 275-1450
Fax: (585) 756-7780
Ethan_Cohen@urmc.rochester.edu

Michael A. O'Reilly, Ph.D.
Department of Pediatrics
Box 850
The University of Rochester
School of Medicine and Dentistry
601 Elmwood Avenue
Rochester, NY 14642
Tel: (585) 275-5948
Fax: (585) 756-7780
michael_oreilly@urmc.rochester.edu

**Running Title**: Hyperoxia and proliferation of atrial cardiomyocytes

**ABSTRACT**

Preterm birth increases the risk for pulmonary hypertension and heart failure in adulthood. Oxygen therapy can damage the immature cardiopulmonary system and may be partially responsible for the cardiovascular disease in adults born preterm. We previously showed that exposing newborn mice to hyperoxia causes pulmonary hypertension by 1 year of age that is preceded by a poorly understood loss of pulmonary vein cardiomyocyte proliferation. We now show that hyperoxia also reduces cardiomyocyte proliferation and survival in the left atrium and causes diastolic heart failure by disrupting its filling of the left ventricle. Transcriptomic profiling showed that neonatal hyperoxia permanently suppressed fatty acid synthase (*Fasn*), stearoyl-CoA desaturase 1 (*Scd1*) and other fatty acid synthesis genes in the atria of mice, the HL-1 line of mouse atrial cardiomyocytes and left atrial tissue explanted from human infants. Suppressing *Fasn* or *Scd1* reduced HL-1 cell proliferation and increased cell death while overexpressing these genes maintained their expansion in hyperoxia, suggesting oxygen directly inhibits atrial cardiomyocyte proliferation and survival by repressing *Fasn* and *Scd1*. Pharmacologic interventions that restore *Fasn*, *Scd1* and other fatty acid synthesis genes in atrial cardiomyocytes may thus provide a way of ameliorating the adverse effects of supplemental oxygen on preterm infants.

**Key Words**: Atria; Cardiomyocytes; Fatty Acid Synthesis; Hyperoxia; Proliferation

## INTRODUCTION

Approximately 10% of births occur before 37 weeks of gestation and are thus considered preterm. Children who are born preterm face an increased risk of developing airway hyperreactivity, chronic wheezing, emphysema and other respiratory diseases as children and young adults than those born at term (1-5). Now that more and more severely preterm infants are reaching adulthood, it is becoming clear that these individuals are also predisposed to pulmonary vascular disease and heart failure (6, 7). Most strikingly, people who were born extremely preterm are 4.6 times more likely to develop pulmonary hypertension and 17 times as likely to suffer heart failure as young adults than people who were born at term (8). While prior studies have reported a loss of pulmonary capillaries, altered ventricular shape and decreased aortic size in young adults born preterm (9-13), the root causes of pulmonary hypertension, heart failure and other cardiovascular diseases in the survivors of preterm birth remain poorly understood. Recent echocardiographic, magnetic resonance, and CT imaging studies indicate that preterm infants have larger left atria and lower diastolic function than term infants (14-17). These changes may be an early and direct response to oxygen exposure because diastolic heart failure has been seen in preterm infants on supplemental oxygen therapies (18).

We and other investigators have been using rodents to understand how early-life exposure to high levels of oxygen (hyperoxia) causes cardiovascular disease. In our model, newborn mice are exposed to room air or hyperoxia (100% oxygen) from birth to postnatal day (PND) 4 and recovered in room air. Mice exposed to neonatal hyperoxia develop pulmonary diseases like those of former preterm infants, including alveolar simplification non-atopic airway hyperreactivity (19) and reduced lung function (20). They also have persistent inflammation and develop fibrotic lung disease after influenza A infection (21, 22). Additionally, hyperoxia-exposed mice develop pathological symptoms of pulmonary hypertension that include pulmonary capillary rarefaction, right ventricular hypertrophy, and a 50% mortality by one year of age (23). Other investigators have similarly observed cardiovascular disease, including right ventricular hypertrophy, hypertension, capillary rarefication and other types of vascular dysfunction, in animals exposed to neonatal hyperoxia (24-28). Together, these findings

demonstrate that neonatal hyperoxia can cause pulmonary hypertension and other cardiovascular diseases in adult rodents.

We recently reported that hyperoxia inhibits the proliferation of the cardiomyocytes wrapping the pulmonary vein and prevents them from expanding to cover its distal branches within the growing lungs of neonatal mice (29). Since these cells form a contractile sleeve around the pulmonary vein and extending into the left atria, the early loss of these cells may increase the force needed to drive pulmonary circulation and thus contribute to the development of pulmonary venous congestion and heart failure in aged hyperoxia-exposed mice (30). Herein, we report that neonatal hyperoxia inhibits the proliferation of left atrial cardiomyocytes by suppressing genes required for the *de novo* synthesis of fatty acids. Failure to expand these cells results in hypoplastic left atria that lose the ability to effectively fill the left ventricle as mice age, a finding that may help explain the pathogenesis of diastolic heart failure in the survivors of preterm birth.

## RESULTS

***Neonatal hyperoxia inhibits left atrial cardiomyocyte proliferation.*** We previously showed that hyperoxia causes a loss of the cardiomyocytes wrapping the pulmonary vein by inhibiting their proliferation (29). Since the pulmonary vein cardiomyocytes are contiguous with the left atria, we investigated whether neonatal hyperoxia altered left atrial morphology. Counterintuitively, H&E staining revealed that the left atria of mice exposed to neonatal hyperoxia were larger than those of controls on PND4 (dotted lines, **Figure 1A, B**). However, co-staining for the cardiomyocyte marker cardiac tropoinin T (TNNT2) and 4',6-Diamidine-2'-phenylindole dihydrochloride (DAPI) showed the number of nuclei per $mm^2$ of TNNT2+ myocardium is reduced in the left atria of PND4 hyperoxia-exposed mice relative to controls (**Figure 1C**). The left atria of mice exposed to neonatal hyperoxia remained larger and continued to have fewer nuclei in TNNT2+ regions of the left atria than controls on postnatal day (PND) 56 (**arrows, Figure 1D-F**) and 365 (**arrows, Figure 1G-I**). Sectioned hearts of PND4 hyperoxia-exposed and room air control mice were next stained for TNNT2 and the mitosis marker phosphorylated histone H3 (pHH3) or cleaved caspase 3 (cl-CASP3), which labels apoptotic cells. Fewer pHH3+ (**arrows, Figure 2A-C**) and more cl-CASP3+ (**arrows, Figure 2D-F**) cardiomyocytes were observed in the left atria of mice exposed to neonatal hyperoxia than controls. Together, these data suggest that neonatal hyperoxia reduced the proliferation and survival of left atrial cardiomyocytes.

***Neonatal hyperoxia causes diastolic dysfunction in adult mice***. To determine how neonatal hyperoxia affects adult heart function, echocardiography was first performed on five PND56 mice who were exposed to room air or hyperoxia between PND0-4 and an equal number of room air controls (**Supplemental Table 1**). Hyperoxia did not affect left ventricular systolic function on PND56 but the calculated mass of the left ventricular wall was lower in hyperoxia-exposed mice than controls. Since a prior study showed hyperoxia reduced ventricular cardiomyocyte proliferation (31), the reduced density of the left ventricular wall observed by echocardiography may reflect lower densities of cardiomyocytes in the left ventricular myocardium. Doppler imaging was used to measure the maximum velocity (Vmax) of blood flowing across the mitral valve during early diastole when the left ventricle relaxes (E-peak)

and late diastole when the left atrium contracts (A-peak). While hyperoxia did not affect either the E- or A-peak Vmax at this age, three of the five hyperoxia-exposed mice had E/A ratios > 2, which is above normal range in humans and mice (32-34).

Cardiac function was next examined in 10 hyperoxia-exposed and 8 room air control mice on PND365 to determine how the effects of neonatal hyperoxia progress with age (**Supplemental table 2**). Four of the ten hyperoxia-exposed mice examined at this age had E/A ratios > 2 like those observed on PND56. Moreover, the mean E/A ratio was higher in hyperoxia-exposed mice than controls on PND365 (**Figure 3A**), although the p-value for this change was slightly above the threshold for significance (unpaired t-test, p=0.051). Interestingly, mean A-peak Vmax was lower in hyperoxia exposed mice than controls at this age while E-peak Vmax was unaffected (**Figure 3B, C**). The ratio of E-peak velocity to mitral annular velocity (E/e'), an indicator of left atrial pressure in early diastole, was also unaffected (room air -32.34 +/- 8.36, n=8; hyperoxia -30.33 +/- 5.92, n=10; p=0.56). Neonatal hyperoxia may thus specifically disrupts the later active phase of diastole, which is driven by atrial contraction, without affecting early diastole, which is driven by ventricular relaxation. Ejection fraction and fractional shortening were also significantly reduced in PND365 hyperoxia-exposed mice relative to controls (**Figure 3D, E**). Neonatal hyperoxia did not significantly affect mean systolic volume of the left ventricle but the two mice with the highest E/A ratios had hearts with much higher left ventricular systolic volumes than controls that were identified as statistical outliers (**arrows, Figure 3F**). The ventricular dilation in the most severely affected mice may help maintain cardiac output in the setting of diastolic dysfunction. In support of this idea, the 2 hyperoxia-exposed mice with the highest E/A ratios and systolic volumes also had higher diastolic volumes, stroke volumes and cardiac outputs than the remaining hyperoxia-exposed mice (**grey circles, Figure 3G-I**). The mean diastolic volume, stroke volume and cardiac output of the remaining mice were also reduced in the remaining mice exposed to neonatal hyperoxia relative to those exposed to room air when these 2 individuals were excluded from the analysis (**white circles, box plots and p-values, Figure 3G-I**). Together, these data suggest neonatal hyperoxia causes mice to develop diastolic dysfunction as adults (PND56) that progresses to heart failure by middle age (PND365).

**Neonatal hyperoxia inhibits the *de novo* fatty acid synthesis pathway in the atria of mice.**

An Affymetrix array was used to identify hyperoxia-induced changes in gene expression responsible for the inhibition of left atrial cardiomyocyte proliferation. RNA was isolated from the atria of 4 hyperoxia-exposed and 3 room air control mice on PND4 and hybridized to the array. Out of 39,000 transcripts examined, only 158 differed by ≥ 1.5-fold with a p-value < 0.05 and false discovery rate < 0.3 (**Figure 4A**). Neonatal hyperoxia increased expression of 53 genes (**Supplemental Table 3**) and inhibited expression of 105 genes (**Supplemental Table 4**). Gene ontology (GO) analysis identified several overlapping sets of genes involved in biosynthetic processes, monocarboxylic acid metabolism, lipid metabolic processes and the regulation of lipid metabolism (**Figure 4B**). The genes involved in fatty acid metabolism that were upregulated in the atria of hyperoxia-exposed mice relative to controls included peroxisome proliferator-activated receptor gamma coactivator 1-alpha (*Ppargc1α*), a transcriptional co-regulator that binds to peroxisome proliferator-activating receptor $\alpha$ and other transcription factors to promote mitochondrial biogenesis (35). Hyperoxia also upregulated acetyl-CoA carboxylase 2 (*Acacb*), a mitochondrial localized isoform of acetyl-CoA carboxylase that produces malonyl-CoA for mitochondrial biogenesis and regulation of β-oxidation (36), hydroxyacyl-CoA dehydrogenase trifunctional multienzyme complex subunit alpha (*Hadha*), part of the mitochondrial complex that catalyzes the β-oxidation of long-chain fatty acids (37), and lipoprotein lipase (*Lpl*), which cleaves lipids from dietary lipoproteins (38).

Neonatal hyperoxia reduced expression of several other genes involved in fatty acid metabolism. These included the core enzymes in the *de novo* fatty acid synthesis pathway such as solute carrier family 25 member 1 (*Slc25a1*), the channel that transports citrate produced by the TCA cycle out of the mitochondria and into the cytoplasm (39, 40), ATP-citrate lyase (*Acly*), the enzyme that converts cytoplasmic citrate to acetyl-CoA (41), and acetyl-CoA carboxylase 1 (*Acaca*), the cytoplasmic isoform of acetyl-CoA carboxylase that produces malonyl-CoA for fatty acid synthesis (42). In addition, hyperoxia reduced mRNA for *fatty acid synthase* (*Fasn*),the enzyme that synthesizes the 16-carbon

saturated fatty acid palmitate from acetyl-CoA and malonyl-CoA (43); *elongation of very long chain fatty acids 6* (*Elovl6*), the enzyme that extends palmitate to produce the 18 carbon saturated fatty acid stearate (44); and *stearoyl-CoA desaturase 1* (*Scd1*), which convert palmitate and stearate to the mono-unsaturated fatty acids palmitoleate and oleate (45), and *thyroid hormone-inducible hepatic protein* (*Thrsp*), which binds FASN and increases its activity (46). Neonatal hyperoxia also downregulated cell death inducing *DFFA like effector c* (*Cidec*), a protein required for the storage of triglycerides as lipid droplets (47), and *adiponectin* (*Adipoq*), an adipokine that protects cardiomyocytes from oxidative stress and apoptosis following ischemic injury (48).

The reduced expression of fatty acid synthesis genes in the atria of mice that were exposed to neonatal hyperoxia was intriguing since this pathway is required for the proliferation and survival of both cancerous and non-cancerous cells (49-53). The expression of fatty acid synthesis genes was thus examined in an independent set of mice to confirm to confirm neonatal hyperoxia suppresses their expression in the atria. Quantitative reverse transcription PCR (qRT-PCR) showed *Slc25a1*, *Acly*, *Acaca*, *Fasn*, *Scd1* and *Thrsp* were all expressed at lower levels in the atria of PND4 mice exposed to neonatal hyperoxia mice than in those of controls (**Figure 4C**). Mean expression of Elovl6 was also lower in hyperoxia-exposed mice relative to controls but the p-value for this change was above the threshold set for significance (p=0.065). In contrast, none of these genes were significantly affected in the ventricles on PND4 (**Figure 4D**). *Acacb* was examined in the hearts of hyperoxia exposed mice but the increased expression in our microarray was not significance in the atria or ventricles of hyperoxia-exposed mice by qRT-PCR. Since mice exposed to hyperoxia are returned to room air on PND4, we investigated when expression of these genes returned to control levels. Surprisingly, mRNA for *Slc25a1*, *Acly*, *Acaca*, *Fasn*, *Scd1*, *Thrsp* and *Elovl6* remained suppressed on PND56 (**Figure 4E**). These changes were again specific for the atrium and the expression of *Slc25a1, Acly, Acaca, Acacb, Thrsp, Fasn,* and *Scd1* in the ventricle was unaffected on PND56, while *Elovl6* was not detected (**Figure 4F**). Hyperoxia thus permanently suppresses fatty acid synthesis genes in the atria but not ventricles.

Immunohistochemistry was used to confirm that neonatal hyperoxia inhibited FASN and SCD1 protein in left atrial cardiomyocytes. Staining for FASN (**red, Figure 5A, B**) and TNNT2 (**green, Figure 5A, B**) detected FASN in the atrial (**arrows**) and ventricular (**arrowheads**) cardiomyocytes of PND4 mice exposed to room air. In contrast, FASN staining was reduced in the left atrial cardiomyocytes of hyperoxia-exposed mice (**Figure 5C**) but unaffected in ventricular cardiomyocytes. Staining for SCD1 (**red, Figure 5D, E**) and TNNT2 (**green, Figure 5D, E**) showed that SCD1 was similarly reduced in left atrial cardiomyocytes of PND4 mice exposed to neonatal hyperoxia relative to controls (**arrows, Figure 5D-F**). As observed for FASN, SCD1 levels were less affected in the ventricles of hyperoxia-exposed and room air control mice (**arrowheads in Figure 5D, E**).

***Hyperoxia inhibits fatty acid synthesis genes and proliferation in the HL-1 line of immortalized murine atrial cardiomyocytes.*** The HL-1 line of immortalized atrial cardiomyocytes was used to examine the direct effects of hyperoxia on fatty acid synthesis genes (54). Cells were grown in room air (21% O2, 5% CO2) or hyperoxia (95% O2, 5% CO2) for 24 or 48 hours before *Fasn* and *Scd1* mRNA were quantified by qRT-PCR (**Figure 6A**). Relative to cells grown in room air, *Fasn* and *Scd1* were reduced in HL-1 cells after 48 hours in hyperoxia. Interestingly, while *Scd1* was lower in HL-1 cells after 24 hours of hyperoxia, *Fasn* was unaffected. However, this difference in timing is unlikely to reflect a regulatory hierarchy between genes because *Scd1* knockdown does not affect *Fasn* expression (Cohen et al., unpublished observation). Hyperoxia can thus directly affect fatty acid synthesis genes in atrial cardiomyocytes without the need for other cell types.

To determine if the suppression of fatty synthesis genes in hyperoxia treated HL-1 cells correlates with reduced proliferation, asynchronously dividing HL-1 cells were plated at equal density and cultured in room air or hyperoxia for 0, 12, 24, 36 and 48 hours before being stained with DAPI and counted. HL-1 cells expanded continuously for 48-hours in room air (**Figure 6B**). In contrast, HL-1 cells grown in hyperoxia expanded slower than controls for the first 24 hours, plateaued from 24 to 36 hours and then

declined in numbers from 36 to 48 hours. These data indicate that hyperoxia directly represses proliferation and fatty acid synthesis genes in HL-1 cells as it does in the atria of mice.

***Fasn* and *Scd1* are required for the proliferation and survival of HL-1 atrial cardiomyocytes**. To determine if fatty acid synthesis is required for atrial cardiomyocyte proliferation, HL-1 cells were transfected with non-targeting (N.T.) siRNA and siRNA for *Fasn* or *Scd1* and grown in room air for 72 hours. Quantitative RT-PCR revealed that *Fasn* and *Scd1* mRNA were reduced around 75% and 90% in cells transfected with *Fasn* and *Scd1* siRNA, respectively, when compared to N.T. siRNA transfected controls (**Figure 6C, D**). Asynchronously dividing *Fasn, Scd1* and N.T. siRNA treated HL-1 cells were then plated at equal numbers and counted at 12-hour intervals (**Figure 6E, F**). Cells transfected with *Fasn* and *Scd1* siRNA grew slower than N.T. siRNA transfected controls over 48 hours.

To confirm *Fasn* and *Scd1* are required for HL-1 cell proliferation, cells were treated with DMSO as a vehicle control, the FASN inhibitor G28UCM at 10μM or the SCD1 inhibitor A939572 at 10nM (Tocris Biosciences) and grown in room air (**Supplemental Figure 1**). While cells in control media grew continuously for 72 hours, cells in A939572 plateaued after 24 hours and cells in G28UCM grew slower than controls during the first 24 hours and then declined in numbers from 24 and 72 hours. To specifically examine the effects of *Fasn* and Scd1 knockdown on proliferation, *Fasn, Scd1* and N.T. siRNA transfected cells were grown for 23 hours, treated with EdU for 1 hour, fixed and stained with an anti-EdU antibody and DAPI. The fraction of EdU+ cells was reduced in *Fasn* and *Scd1* siRNA treated cells relative to controls (**Figure 6G**). Propidium iodide (PI) exclusion assays were performed to determine if *Fasn* and *Scd1* were required for HL-1 cell survival. The percentage of PI+ cells was significantly higher in *Scd1* siRNA transfected cells than controls. The percentage of PI+ cells was also higher in cells transfected with *Fasn* siRNA than controls, but the p-value of this change was slightly below the threshold for statistical significance (0.051). Together, these data show that the *Fasn and Scd1* are required for atrial cardiomyocyte proliferation and survival.

***Fasn* and *Scd1* overexpression restores proliferation of HL-1 atrial cardiomyocytes in hyperoxia.**

We next sought to determine how *Fasn* and *Scd1* overexpression would affect atrial cardiomyocyte proliferation in hyperoxia. Cells were transfected with *Fasn* and *Scd1* expression vectors (*CMV-Fasn* and *CMV-Scd1*, respectively) as well as empty expression vector. After 24 hours, cells were replated at equal density and grown in room air or hyperoxia for 0, 12 and 24 hours before being stained and counted. Cells transfected with *CMV-Fasn* expressed approximately two-fold more *Fasn* than empty vector transfected cells (**Figure 7A**). As expected, control transfected cells grew slower in hyperoxia than in room air (**Figure 7B**). However, *CMV-Fasn* transfected cells grew at the same rate as control cells grew in room air, regardless of whether they were in room air or hyperoxia. Cells transfected with *CMV-Scd1* expressed approximately 60-fold more *Scd1* than controls (**Figure 7C**) and grew faster than control cells in room air and hyperoxia (**Figure 7D**). *Fasn* and *Scd1* overexpression thus partially restores HL-1 cell growth in hyperoxia.

To specifically examine the effects of *Fasn* and *Scd1* overexpression on proliferation, HL-1 cells were transfected with control, *Fasn* and *Scd1* plasmids, grown in room air or hyperoxia for 23 hours and treated with EdU to label cells in S-phase (**Figure 7E**). While numbers of EdU+ cells were unaffected by *Fasn* and *Scd1* overexpression in room air, more *Fasn* and *Scd1* overexpressing cells were EdU+ in hyperoxia than controls. Cells transfected with control, *Fasn* and *Scd1* plasmids were also grown in room air or hyperoxia for 48 hours and subject to PI exclusion assays to determine if *Fasn* and *Scd1* promote survival in hyperoxia (**Figure 7F**). Consistent with the increased numbers of cl-CASP3+ cells in the atria of PND4 hyperoxia-exposed mice, 48 hours of hyperoxia increased the percentage of control transfected cells stained by PI. While *Scd1* overexpression caused a modest reduction in the numbers of PI+ cells in room air, *Fasn* did not. However, *Fasn* and *Scd1* overexpressing cells were both less likely to be PI+ in hyperoxia than controls. Restoring *Fasn* and *Scd1* expression can thus partially restore the survival and proliferation of atrial cardiomyocytes in hyperoxia.

If *Fasn* and *Scd1* promote the growth of HL-1 cells in hyperoxia by increasing the supply of their products, adding exogenous fatty acids to the culture media may mimic their effects. Cells were thus plated in media containing increasing amounts of BSA-conjugated palmitate (**Figure 7G, H**) or oleate (**Figure 7I, J**) and grown in room air (**Figure 7G, I**) or hyperoxia (**Figure 7H, J**) for 36 hours. In room air, cells grew at equal rates in media containing low and medium levels of palmitate and Oleate conjugated BSA as they did in media containing unconjugated BSA. In contrast, high concentrations of palmitate and oleate slowed the growth of cells in room air relative to controls. High levels of palmitate and oleate similarly slowed HL-1 cell growth in hyperoxia relative to controls. As seen in room air, low and medium concentrations of oleate did not affect HL-1 cell growth in hyperoxia. However, HL-1 cells treated with low and intermediate levels of palmitate grew slower in hyperoxia than cells in control media, suggesting hyperoxia enhances the effects of palmitate-BSA on their expansion. Palmitate and oleate are thus not sufficient for the effects of *Fasn* and *Scd1* overexpression on atrial cardiomyocyte growth in hyperoxia.

**Hyperoxia does not reduce SREBF1 protein in atrial cardiomyocytes.** Genes in the *de novo* fatty acid synthesis pathway are regulated by sterol-response element binding factor 1 (SREBF1), a transcriptional master regulator of lipogenesis (55). HL-1 cells were thus transfected with plasmid that expresses human SREBF1 under the control of the *CMV* promoter (*CMV-Srebf1*) or empty vector and grown in hyperoxia or room for 36 hours. Performing qRT-PCR with a primer pair recognizing both human and mouse *Srebf1* mRNA showed cells transfected with *CMV-Srebf1* expressed nearly twice as much *Srebf1* than control cells (**Supplemental Figure 2A**). *CMV-Srebf1* transfected cells grew slower in room air than those transfected with empty vector (**Supplemental Figure 2B**). However, while control transfected cells growth arrested after 12 hours in hyperoxia, *CMV-Srebf1* transfected cells continued proliferating in hyperoxia up to 36 hours (**Supplemental Figure 2C**).

To determine if hyperoxia suppresses fatty acid synthesis genes by reducing SREBF1 protein, western blotting for SREBF1 was performed on HL-1 cells grown in room air or hyperoxia for 48 hours

(**Supplemental Figure 2D**). Two bands of SREBF1 protein were detected in hyperoxia- and control-treated HL-1 cells, a 120kd band representing full length inactive SREBF1 within the golgi membrane, and a 55kd band representing the amino-terminus of SREBF1, which localizes to the nucleus after cleavage. Despite the reduced expression of *Fasn, Scd1* and other fatty acid genes in hyperoxia-treated cells, hyperoxia does not alter the levels of either band of SREBF1 protein (**Supplemental Figure 2F, G**). Lysates of left atria from individual PND4 hyperoxia-exposed and control mice were also western blotted for SREBF1 protein (**Supplemental Figure 2E**). Surprisingly, despite having lower levels of fatty acid synthesis genes than controls, the left atria of PND4 hyperoxia-exposed mice had higher levels of both forms of SREBF1 than controls (**Supplemental Figure 2H, I**). Therefore, hyperoxia is unlikely to reduces fatty acid synthesis in atrial cardiomyocytes by reducing SREBF1 protein in these cells.

***Hyperoxia inhibits fatty acid synthesis genes and proliferation in human left atrial tissue explanted from infant donors.*** To determine if changes observed in mice occur in humans, left atrial tissue from term infants who died shortly after birth due to anencephaly was obtained from the Biorepository for Investigation of Neonatal Diseases of the Lung (BRINDL) at the University of Rochester. The muscle was separated from surrounding tissue, cut into ~1 $mm^3$ cubes, grouped and cultured in room air or hyperoxia for 24 hours before being used for qRT-PCR or immunostaining. While hyperoxia did not alter the levels of *Fasn* mRNA, *Scd1* expression was lower in hyperoxia-exposed explants than controls (**Figure 8A**). Immunological staining showed that SCD1 protein localized to TNNT2+ cardiomyocytes in explants exposed to room air but not in those exposed to hyperoxia (**arrows, Figure 8B, C**). Sectioned explants were stained for the proliferation marker Ki-67 and TNNT2 to determine if hyperoxia reduced the proliferation of human left atrial cardiomyocytes. Ki67+ nuclei were more frequently observed in the TNNT2+ cardiomyocytes of control explants than in those exposed to neonatal hyperoxia (**arrows, Figure 8D, E**). Hyperoxia thus suppresses fatty acid synthesis genes and proliferation in human left atrial cardiomyocytes as it does in mice.

## DISCUSSION

There is a significant need to understand why high oxygen exposure at birth is a risk factor for adult cardiovascular disease. We previously showed that neonatal hyperoxia causes pulmonary hypertension in adult mice and that this phenotype was preceded by a loss of the cardiomyocytes surrounding the pulmonary vein due to reduced proliferation (29). We now extend these findings by showing hyperoxia similarly inhibits the postnatal proliferation of left atrial cardiomyocytes and causes the myocardium of this chamber to be hypoplastic. Despite having fewer cardiomyocytes per unit area, the left atria of hyperoxia-exposed mice were larger than controls, suggesting that the remaining cardiomyocytes hypertrophy to compensate for reduced numbers. Pathology was first seen on PND56 when most of the hyperoxia-exposed mice examine had E/A ratios > 2. By PND365 the mean E/A ratio was higher in mice exposed to neonatal hyperoxia than controls. The velocity of flow across the mitral valve during atrial contraction was also lower in hyperoxia-exposed mice than controls, suggesting hyperoxia reduced left atrial contractility by this age. Interestingly, the two mice with the highest E/A ratios (>5) had left ventricles that were larger than controls during both systole and diastole. The left ventricular dilation in these mice may be adaptive since it would raise cardiac output in the presence of diastolic dysfunction, reduced fractional shortening and lower ejection fraction. In support of this idea, excluding the two mice with the highest E/A ratios from our analyses diastolic volume, stroke volume and cardiac output were lower in the remaining hyperoxia-exposed mice than controls. Mice exposed to hyperoxia during early postnatal life thus develop diastolic dysfunction and heart failure as adults.

Affymetrix arrays, qRT-PCR and immunohistochemistry revealed that neonatal hyperoxia inhibited genes needed for fatty acid synthesis in the atrial but not ventricular cardiomyocytes of mice. These included *Fasn* and *Scd1*, which are elevated in highly proliferative tumors, sufficient to drive the expansion of non-cancerous cells when overexpressed and required for the proliferation and survival of non-cardiac cells (49, 53, 56-60). We thus explored whether the repression of *Fasn* and *Scd1* is responsible for the reduced proliferation of left atrial cardiomyocytes in mice exposed to neonatal hyperoxia. Left atrial cardiomyocytes can be isolated from neonatal mice but the yield is low, and the

resulting cells lose their proliferative capacity quickly in culture, making it difficult to examine how genetic manipulations affect their expansion. The HL-1 line of immortalized atrial cardiomyocytes was thus chosen to model the effects of hyperoxia on neonatal atrial cardiomyocytes since these cells are differentiated and contractile but still metabolically immature and proliferative (54, 61, 62). Consistent with the loss of atrial CM proliferation and survival in hyperoxia-exposed mice, exposing HL-1 cells to hyperoxia for 48 hours suppressed *Fasn* and *Scd1* and reduced proliferation and survival. Inhibitors and siRNAs for *Fasn* and *Scd1* also reduced HL-1 cell proliferation and survival while overexpressing these genes partially restored growth in hyperoxia. The repression of *Fasn* and *Scd1* may therefore mediate the inhibitory effects of neonatal hyperoxia on the postnatal proliferation and survival of left atrial cardiomyocyte.

Surprisingly, adding palmitate and oleate to the culture media was not sufficient to reproduce the effects of *Fasn* and *Scd1* overexpression on the expansion of HL-1 cells in hyperoxia. It is possible that fatty acids produced *de novo* are preferred over exogenous fatty acids for synthesizing phospholipids and other components of new membranes for dividing cells. Alternatively, fatty acid synthesis may prevent potentially toxic metabolic precursors from accumulating. Chemical inhibition and siRNA-mediated knockdown of FASN inhibits oxidative phosphorylation in immortalized melanocytes (49). This loss of mitochondrial function was partially due to the accumulation of malonyl-CoA, which inhibits the transports fatty acids into mitochondria at high concentrations. FASN inhibition also reduces mitochondrial membrane potential ($\Delta\Psi m$) and increases production of reactive oxygen species (63, 64). SCD1 inhibition similarly disrupts mitochondrial function, increases ROS and induces apoptosis in many cells including neonatal ventricular cardiomyocytes (65, 66). Reduced SCD1 function also activates AMP-dependent protein kinase (AMPK) in many contexts, including the hearts of *Scd1* knockout mice (45, 67, 68). AMPK phosphorylates and inhibits the pro-proliferative kinase mammalian target of rapamycin (mTOR) and thus inhibits tumor cell proliferation and survival (69). AMPK also reduces fatty acid synthesis through inhibitory phosphorylation of ACACA as well as SREBF1 (70) and may thus play a role in the hyperoxia-induced suppression of fatty acid synthesis in atrial cardiomyocytes.

Recent echocardiographic, magnetic resonance and CT imaging studies indicate that preterm infants have larger left atria and lower diastolic function than term infants (14-17), suggesting that the heart failure among young adults born preterm has developmental origins. Serum from preterm infants was shown to have higher malonyl-carnitine and lower palmitoyl-carnitine levels than serum from term infants (71), suggesting preterm birth and reduced FASN activity may be linked. Preterm infants often require mechanical ventilation, steroids, and other interventions that make it difficult to identify direct effects of supplemental oxygen on cardiovascular health. We thus sought to determine if hyperoxia suppresses fatty acid synthesis genes and proliferation in explanted human left atrial tissue. Hyperoxia reduced *Scd1* expression and the numbers of Ki67+ cardiomyocytes in human atrial explants, confirming hyperoxia represses at least one major component of the fatty acid synthesis pathway as well as proliferation in human left atrial cardiomyocytes. These data suggest that the response of left atrial tissue from newborn human to hyperoxia parallels that of mice and HL-1 cells and that reduced fatty acid synthesis underlies the cardiovascular disease in preterm infants.

Exposure to neonatal hyperoxia did not suppress fatty acid synthesis genes in the ventricles of mice as it did in the atria. Since the left atrium is the first chamber to encounter oxygen-rich blood from the lungs, left atrial cardiomyocytes may have evolved to have a different response to hyperoxia than ventricular cardiomyocytes. The levels *Fasn*, *Scd1* and other fatty acid synthesis genes were also lower in the ventricles of both hyperoxia exposed and room air control mice at all times examined, suggesting that fatty acid synthesis may be less important for proliferation and survival of ventricular than atrial cardiomyocytes. The suppression of ventricular cardiomyocyte proliferation was hypothesized to reflect a role for oxygen in promoting their terminal differentiation and maturation (31). However, in our model, *Fasn*, *Scd1* and other fatty acid synthesis genes continue to be suppressed in the atria of mice exposed to hyperoxia even after they are returned to room air. If hyperoxia accelerated the normal differentiation of atrial cardiomyocytes as proposed, fatty acid synthesis genes should return to similar levels in the atria of hyperoxia-exposed and control mice as the atrial cardiomyocytes of control mice matured.

Exposure to hyperoxia in early neonatal life thus permanently reprograms atrial cardiomyocytes metabolism in a maladaptive fashion that may contribute to the long-term effects of neonatal hyperoxia on cardiovascular health. It is unclear if similar persistent molecular changes take place in ventricular cardiomyocytes.

Despite the strength of the data presented, it is important to acknowledge the limitations of our studies. HL-1 cells are a pure population of proliferative atrial cardiomyocytes that can be used to test the functional relationship between hyperoxia and fatty acid synthesis genes. However, these cells have been immortalized with the SV40 T-antigen and may not faithfully recapitulate the response of primary atrial cardiomyocytes to hyperoxia or the complex interactions between cells within the left atrium. The left atrial tissue used to demonstrate that hyperoxia affects fatty acid synthesis and cardiomyocytes proliferation in humans was from anencephalic infants that were born at term and died shortly thereafter instead of preterm infants. Since oxygen sensitivity is likely to change over the course of gestation, the response of human left atrial explants may not accurately reflect how left atrial cardiomyocytes respond to supplemental oxygen in preterm infants. Moreover, hyperoxia did not suppress *Fasn* in explanted human atrial tissue as it did in the atria of mice. Since, one day of hyperoxia was insufficient to repress *Fasn* in HL-1 cells, prolonged exposure to hyperoxia may be needed suppress *Fasn* in atrial explants. Alternatively, ex vivo studies may not recapitulate the effects of hyperoxia seen in vivo. Future studies will be required to determine if restoring fatty acid synthesis will alleviate the effects of neonatal hyperoxia on left atrial cardiomyocytes in the hearts of mice or if fatty acid synthesis genes are reduced in banked heart tissue from preterm infants.

In conclusion, the data herein suggest exposure to hyperoxia in early postnatal life initiates the development of adult diastolic dysfunction by permanently suppressing *Fasn*, *Scd1* and other genes needed for fatty acid synthesis as well as cardiomyocyte proliferation and survival within the myocardia of the left atrium. Although the remaining cardiomyocytes hypertrophy to compensate for the reduced numbers of cells, the reduced A-peak velocities in aged mice exposed to neonatal hyperoxia suggest

these cells lose contractility over time. Moreover, since adult cardiomyocytes use fatty acids for 70% of the ATP used for contractility (72), the long-term suppression of *Fasn, Scd1* and other fatty acid synthesis genes may affect the functionality of the remaining cardiomyocytes after they have stopped proliferating and further contribute to the diastolic heart failure. Agonists for nuclear hormone receptors that work with SREBF1 to induce lipogenesis, such as liver X receptor (LXR), and peroxisome proliferator-activated receptor gamma (PPARG) are currently available (73-77). Future studies will thus be needed to determine if these compounds can be used to protect or restore the postnatal proliferation and survival of atrial cardiomyocytes in mice exposed to hyperoxia and potentially lead to novel therapies to prevent diastolic heart failure in individuals who were born preterm.

## MATERIALS AND METHODS

*Mice and hyperoxia.* C57BL/6J mice were purchased from The Jackson Laboratories (Bar Harbor, MA) and maintained as an inbred colony. Mice were exposed to humidified room air (21% oxygen) or hyperoxia (100% oxygen) between postnatal days 0-4 (22). Some mice exposed to hyperoxia were returned to room air. Dams were cycled between room air and hyperoxia every 24 hours to reduce oxidant injury. The mice were provided food and water *ad libitum* and housed in micro-isolator cages in a pathogen-free environment. Since we have not observed differences in the response of male and female mice to hyperoxia in prior studies, male and female mice were both used in experiments performed on PND4. However, all male mice were used to examine the effects of neonatal hyperoxia on cardiac function on PND56 and PND365 to prevent sex specific differences in ventricular measurements from masking potential effects of hyperoxia.

*Echocardiography.* To assess cardiac function, mice were anesthetized with isoflurane and subject to transthoracic echocardiography using a VisualSonics Vevo 3100 with a 40 MHz transducer. M-mode scans along the short axis of the LV were acquired at the level of the papillary muscle to determine the internal diameters and volumes of the left ventricle in systole and diastole, widths of the anterior and posterior walls of the left ventricle, mass of the free wall of the left ventricle, heart rate, fractional

shortening, ejection fraction, stroke volume and cardiac output. Doppler images of flow across the mitral valve were used to determine the Vmax during the E- and A-peaks as well as the E/A ratio. Tissue doppler images were used to determine e' and the E/e' ratios of mice examined on PND365. Five neonatal hyperoxia-exposed and five control mice were examined on PND56. Ten hyperoxia-exposed and eight control mice were examined on PND365. F-tests were used to determine if the variance between values for hyperoxia-exposed and control mice had equal or unequal variance and the appropriate unpaired t-test with $p < 0.5$ used to identify statistically significant differences in mean values for hyperoxia-exposed and control mice. Measurements were made by the staff of the Microsurgery and Echocardiography Core at the Aab Cardiovascular Research Institute, who were blinded to the treatment of the animals.

*Affymetrix Arrays and Analysis.* Total RNA was isolated from the atria of PND4 mice exposed to room air or hyperoxia using Trizol (ThermoFisher Scientific, Waltham, MA) and its integrity validated using an Agilent Bioanalyzer (Agilent Technologies, Santa Clara, CA). The RNA was converted to cDNA, biotinylated with Ovation kits from NuGEN (San Carlos, CA) and hybridized to the Affymetrix mouse genome 430 2.0 array (Affymetrix, Santa Clara, CA). Each array was probed with RNA from an individual mouse. Arrays were stained with streptavidin-phycoerythrin as recommended. Arrays were scanned for phycoerythrin fluorescence and spot intensities normalized across arrays with the RMA method in the "oligo" package (78). Affymetrix cell file were loaded in R 3.4.3/Bioconductor 3.5 using the oligo package and RMA-normalized. 29290 features that passed filters on mean expression > 3 and total variance > 0.0025 were tested for differential expression with limma (79). A total of 157 genes with FDR-adjusted q-values < 0.30 was tested for enrichment in gene ontology using ClusterProfiler. Complete array datasets were deposited in ArrayExpress under accession E-MTAB-9008.

*Quantitative RT-PCR.* Total RNA was isolated using Trizol, treated with DNase to remove genomic DNA and reverse transcribed using the Maxima First Strand cDNA synthesis kit (ThermoFisher Scientific, Waltham, MA). Quantitative RT-PCR was performed using the primer pairs listed in **Table 4** and iTaq

SYBR Green Master Mix on a CFX384™ Real-Time PCR detection system (Bio-Rad Laboratories, Hercules, CA). Fold changes in gene expression were calculated by the ΔΔCt method using average Ct value for housekeeping genes *Pol2ra*, and *Gapdh* to control for loading. Since data were compiled from multiple runs, sample numbers for each gene depended on availability. PND4 atria and ventricle N = 5 control, 6 hyperoxia-exposed except *Thrsp* and *Elovl6* in the atria, for which N=7. PND56 atria, 4 controls and 4 hyperoxia-exposed for *Scd1*, *Thrsp* and *Elovl6*, while N=5 hyperoxia-exposed mice for *Slc25a1*, *Acly*, *Acaca* and *Acacb*. PND56 ventricles, N = 5 control and 5 experimental for *Slc25a1*, *Acly*, *Acaca* an *Acacb*, while *Fasn*, *Scd1*, *Thrsp* and *Elovl6* were examined in 4 control and 4 hyperoxia-exposed mice. F-tests were used to determine if the values for control and hyperoxia-exposed mice had equal or unequal variance. Unpaired t-tests with p-values < 0.05 indicated significance.

*Tissue processing, histological sectioning, and Immunostaining.* Intraperitoneal injections of Avertin and heparin were used to euthanize mice and prevent clotting, respectively. Hearts were perfused with PBS and 10% neutral buffered formalin (NBF) to remove blood and fix the tissue, respectively and fixed in 4% PFA overnight before being embedded in paraffin, sectioned, and stained as described (20, 80). Sections were stained with hematoxylin and eosin (H&E) and Masson's trichrome to assess morphology. The area of the left atrium was determined for three sections of each heart located near the aortic and mitral valves with ImageJ 2.0/Fiji and averaged for each individual mouse and used as 1 biological replicate. For PND4 and PND56 mice, N=4 controls and 4 hyperoxia exposed mice. For PND365 mice, N=3 controls and 4 hyperoxia exposed mice. To determine the density of cardiomyocytes within the left atrial myocardium, sections were stained for TNNT2 (ThermoFisher Scientific, MA5-12960) and 4', 6-diamidino-2-phenylindole (DAPI). The TNNT2+ areas of each atria were imaged using a Nikon E800 Fluorescence microscope (Microvideo Instruments, Avon, MA) and a SPOT-RT digital camera (Diagnostic Instruments, Sterling Heights, MI) so numbers of DAPI+ nuclei within the TNNT2+ areas in each image could be counted using the find maxima function of ImageJ 2.0/Fiji. For PND4 mice, N = 4 controls and 5 hyperoxia-exposed mice. For PND56 mice, N=3 control and 3 hyperoxia-exposed mice. For PND365 mice, N=4 control and 4 control mice. To determine

numbers of pHH3+ and cl-Casp3+ cardiomyocytes, sections were stained with for pHH3 (Cell Signaling, 9701) or cl-Casp3 (Cell Signaling, 9661) as well as TNNT2, imaged and counted using Image J2.0/Fiji. For pHH3 staining on PND4, N=4 control and 4 hyperoxia exposed mice. For cl-Casp3 staining on PND4, N=4 control and 5 hyperoxia-exposed mice. Antibodies for FASN and SCD1 (ThermoFisher Scientific, PA5-19509 and PA5-17409, respectively) were used to examine protein levels and localizations in PND4 mice. The intensities of FASN and SCD1 staining were determined using the measure tool of Image J 2.0/Fiji. N=5 control and 5 hyperoxia-exposed mice for both FASN and SCD1.

*Culture of immortalized murine atrial cardiomyocytes*. HL-1 cells were cultured in Claycomb media with 100 μM norepinephrine, 300 μM ascorbic acid, 10% fetal bovine serum, 4 mM glutamine and penicillin/ streptomycin (cells and media obtained from Sigma-Aldrich, St. Louis, MO). When indicated, cells were transfected with 30 pMol of pooled siRNA against *Fasn* and *Scd1* (Horizon, L-040091-00 and M-040675-01) per well of a 6-well plate or 3.5 μg of *Fasn* and *Scd1* cDNAs (Horizon, MMM1013-202765185 and MMM1013-202762947) using Lipofectamine RNAiMax or 2000 with a 3:1 ratio of transfection reagent to nucleic acid (ThermoFisher Scientific, Waltham, MA). Cells transfected with 30 pMol non-targeting siRNA and 3.5 μg of empty vector served as controls. The levels of siRNA, DNA and transfection reagents used to transfect cells in other sized cluster plates were scaled according to surface area. For growth assays, cells were plated in 96 well dishes at a density of 5000 cells/well and allowed to attach overnight. Cells were exposed to room air and hyperoxia for 48 hours with plates being fixed at 0, 12, 24 and 48 hours. Fixed cells were stained with DAPI and scanned on a Celigo S Image Cytometer (Nexcelom Bioscience, Lawrence, MA) to count nuclei/well with the associated software. When indicated, 10 mM G28UCM and 10 nM A939657 (Tocris Bioscience, Bristol, UK) were added before exposure to inhibit FASN and SCD1, respectively. Cells treated with DMSO were used as vehicle controls. For EdU incorporation, cells were exposed to room air or hyperoxia for 23 hours before 10 μM 5-ethynyl-2'-deoxyuridine (EdU) was added to the media. Cells were returned to room air or hyperoxia for 1 hour and fixed before EdU+ cells were detected with the Click-IT EdU Cell

Proliferation Kit (ThermoFisher Scientific, Waltham, MA). Cells were co-stained with Hoechst and imaged on an Celigo Image Cytometer to determine percentages of EdU+ cells.

*Western blotting:* HL-1 cells were plated at equal density and cultured in room air or hyperoxia for 48 hours and then lysed in 2x Laemmli buffer (Biorad, 161-0737) containing protease and phosphatase inhibitor cocktail (ThermoFisher Scientific, 78442). The left atria of hyperoxia-exposed and room air control mice were dissected away from the the heart using forceps and lysed in 2x Laemmli buffer with protease/ phosphatase inhibitors as described. Samples were heated at 95 degrees Celsius for 5 minutes, separated by SDS-PAGE and transferred onto PVDF. Membranes were stained with antibody for SREBF1 (Sigma-Aldrich, SAB2102992), HRP-conjugated goat anti-rabbit antibody and SuperSignal West Pico substrate (ThermoFisher, Scientific 34080). Blots were scanned on a Bio-Rad ChemiDoc System and densitometry done with associated software. N=3 independent wells each for room air and hyperoxia exposed cells. N=4 left atria from control mice and 5 left atria from hyperoxia-exposed mice.

*Ex vivo culture of human left atrial tissue*. Tissue from 4 donors with anencephaly who died within 24 hours of birth at 37 weeks and 1 donor with Hirschsprung's and demyelinating disease that died at 3 months of age was used to examine the effects of hyperoxia on *Fasn*, *Scd1* and *Ki67* expression. Explants from these donors and another 2 donors that died after 36 weeks gestation due to anencephaly for which RNA was unavailable were sectioned and used to examine how hyperoxia affects SCD1 and Ki67 staining. In all cases, myocardium was cleaned of surrounding tissue, cut into ~1 $mm^3$ cubes and cultured in EMEM with Insulin-Transferrin-Selenium (ITS). Explants were examined on an inverted microscope with heated stage to confirm they were beating and viable before and after being divided into groups of 10-15 explants and cultured in room air or hyperoxia for 24 hours. After exposure, explants were lysed for RNA extraction and qRT-PCR or fixed for sectioning and immunologic staining. For qRT-PCR studies, fold changes in expression between explants cultured in room air and hyperoxia were calculated for five donors and averaged to report mean fold changes in mRNA levels. One sample

t-tests were used to determine if mean fold changes relative to room air exposed explants in *Fasn* and *Scd1* deviated significantly from one.

*Statistics*. Data was analyzed with JMP12 (SAS Institute, Cary, NC) and graphed with Prism 8 (GraphPad Software, San Diego, CA). Single variant studies were judged using unpaired t-tests. F-tests were used to determine if samples had equal or unequal variance. Simultaneously measured parameters were judged with unpaired t-tests and Holm-Sidak corrections. Studies with more than two experimental conditions were judged using one-way ANOVA with Tukey's multiple comparisons tests. Growth curve and other multivariant data were judged using two-way ANOVA with Sidak multiple comparisons tests or linear regression. In all cases, $p < 0.05$ were considered significant. The statistical analysis of Affymetrix array data and gene expression in human atrial tissue was performed as described in their subsections of the Materials and Methods.

*Study approvals*. Mouse studies were approved by the University Committee on Animal Resources at the University of Rochester (protocol 20070-121R). Human tissue was provided through the federal United Network of Organ Sharing via National Disease Research Interchange (NDRI) and the International Institute for Advancement of Medicine (IIAM) and entered into the NHLBI LungMAP Biorepository for INvestigations of Diseases of the Lung (BRINDL) at the University of Rochester Medical Center overseen by the IRB as RSRB00047606, as described (81, 82).

**AUTHOR CONTRIBUTIONS**

EDC and MAO designed and supervised experiments and wrote the manuscript. GAP, GSP, PSB and ANM helped with experimental design, data analysis and editing. MY and EDC handled mice and collected tissues. GSP collected human samples. ANM analyzed microarray datasets. EDC, MY and ER performed all experiments. EDC and GAP analyzed echocardiography data.

**ACKNOWLEDGEMENTS**

This work was funded in part by National Institutes of Health Grants R01 HL091968 (M.A. O'Reilly), Strong Children's Research Center pilot grant (E.D. Cohen), and a Wine Auction Pilot from the Cardiovascular Research Institute (M.A. O'Reilly and G. Porter). NIH Center Grant P30 ES001247 supported the animal inhalation facility and tissue-processing core. The University of Rochester's Department of Pediatrics provided financial support through the Perinatal and Pediatric Origins of Disease Program and directly to the Pediatric Histology Service. We thank Robert Gelein for maintaining the oxygen exposure facility, Daria Krenitsky for tissue processing, and the University of Rochester's Genomic Research Center for performing microarrays. We thank the donating families, the Research Recovery Organization IIAM, the LungMAP Consortium supported by NHLBI Molecular Atlas of Lung Development Program Human Tissue Core grants (U01HL122700 and U01HL148861) and Heidie Huyck, Cory Poole, and other Pryhuber lab members who prepared the human heart tissue.

## REFERENCES


1. Robin B, Kim YJ, Huth J, Klocksieben J, Torres M, Tepper RS, et al. Pulmonary function in bronchopulmonary dysplasia. *Pediatric pulmonology.* 2004;37(3):236-42.
2. Doyle LW. Respiratory function at age 8-9 years in extremely low birthweight/very preterm children born in Victoria in 1991-1992. *Pediatric pulmonology.* 2006;41(6):570-6.
3. Doyle LW, Faber B, Callanan C, Freezer N, Ford GW, and Davis NM. Bronchopulmonary dysplasia in very low birth weight subjects and lung function in late adolescence. *Pediatrics.* 2006;118(1):108-13.
4. Smith VC, Zupancic JA, McCormick MC, Croen LA, Greene J, Escobar GJ, et al. Rehospitalization in the first year of life among infants with bronchopulmonary dysplasia. *The Journal of pediatrics.* 2004;144(6):799-803.
5. Weisman LE. Populations at risk for developing respiratory syncytial virus and risk factors for respiratory syncytial virus severity: infants with predisposing conditions. *The Pediatric infectious disease journal.* 2003;22(2 Suppl):S33-7; discussion S7-9.
6. Eber E, and Zach MS. Long term sequelae of bronchopulmonary dysplasia (chronic lung disease of infancy). *Thorax.* 2001;56(4):317-23.
7. Bensley JG, De Matteo R, Harding R, and Black MJ. The effects of preterm birth and its antecedents on the cardiovascular system. *Acta obstetricia et gynecologica Scandinavica.* 2016;95(6):652-63.
8. Carr H, Cnattingius S, Granath F, Ludvigsson JF, and Edstedt Bonamy AK. Preterm Birth and Risk of Heart Failure Up to Early Adulthood. *J Am Coll Cardiol.* 2017;69(21):2634-42.
9. Lewandowski AJ, Davis EF, Yu G, Digby JE, Boardman H, Whitworth P, et al. Elevated blood pressure in preterm-born offspring associates with a distinct antiangiogenic state and microvascular abnormalities in adult life. *Hypertension.* 2015;65(3):607-14.
10. Doyle LW, Faber B, Callanan C, and Morley R. Blood pressure in late adolescence and very low birth weight. *Pediatrics.* 2003;111(2):252-7.
11. Lewandowski AJ, Augustine D, Lamata P, Davis EF, Lazdam M, Francis J, et al. Preterm heart in adult life: cardiovascular magnetic resonance reveals distinct differences in left ventricular mass, geometry, and function. *Circulation.* 2013;127(2):197-206.
12. Kowalski RR, Beare R, Doyle LW, Smolich JJ, and Cheung MM. Elevated Blood Pressure with Reduced Left Ventricular and Aortic Dimensions in Adolescents Born Extremely Preterm. *The Journal of pediatrics.* 2016;172:75-80 e2.
13. Edstedt Bonamy AK, Bengtsson J, Nagy Z, De Keyzer H, and Norman M. Preterm birth and maternal smoking in pregnancy are strong risk factors for aortic narrowing in adolescence. *Acta Paediatr.* 2008;97(8):1080-5.
14. Castaldi B, Bordin G, Favero V, Nardo D, Previati F, Salvadori S, et al. Early modifications of cardiac function in preterm neonates using speckle tracking echocardiography. *Echocardiography.* 2018;35(6):849-54.
15. de Waal K, Costley N, Phad N, and Crendal E. Left Ventricular Diastolic Dysfunction and Diastolic Heart Failure in Preterm Infants. *Pediatr Cardiol.* 2019;40(8):1709-15.
16. Burchert H, and Lewandowski AJ. Preterm Birth Is a Novel, Independent Risk Factor for Altered Cardiac Remodeling and Early Heart Failure: Is it Time for a New Cardiomyopathy? *Curr Treat Options Cardiovasc Med.* 2019;21(2):8.
17. Phad NS, de Waal K, Holder C, and Oldmeadow C. Dilated hypertrophy: a distinct pattern of cardiac remodeling in preterm infants. *Pediatr Res.* 2020;87(1):146-52.
18. Hirose A, Khoo NS, Aziz K, Al-Rajaa N, van den Boom J, Savard W, et al. Evolution of left ventricular function in the preterm infant. *J Am Soc Echocardiogr.* 2015;28(3):302-8.
19. Regal JF, Lawrence BP, Johnson AC, Lojovich SJ, and O'Reilly MA. Neonatal oxygen exposure alters airway hyper-responsiveness but not the response to allergen challenge in adult mice. *Pediatric allergy and immunology : official publication of the European Society of Pediatric Allergy and Immunology.* 2014;25(2):180-6.

20. Yee M, Chess PR, McGrath-Morrow SA, Wang Z, Gelein R, Zhou R, et al. Neonatal oxygen adversely affects lung function in adult mice without altering surfactant composition or activity. *American journal of physiology Lung cellular and molecular physiology.* 2009;297(4):L641-9.
21. O'Reilly MA, Marr SH, Yee M, McGrath-Morrow SA, and Lawrence BP. Neonatal hyperoxia enhances the inflammatory response in adult mice infected with influenza A virus. *Am J Resp Crit Care.* 2008;177(10):1103-10.
22. Buczynski BW, Yee M, Martin KC, Lawrence BP, and O'Reilly MA. Neonatal hyperoxia alters the host response to influenza A virus infection in adult mice through multiple pathways. *American journal of physiology Lung cellular and molecular physiology.* 2013;305(4):L282-90.
23. Yee M, White RJ, Awad HA, Bates WA, McGrath-Morrow SA, and O'Reilly MA. Neonatal hyperoxia causes pulmonary vascular disease and shortens life span in aging mice. *The American journal of pathology.* 2011;178(6):2601-10.
24. Yzydorczyk C, Comte B, Cambonie G, Lavoie JC, Germain N, Ting Shun Y, et al. Neonatal oxygen exposure in rats leads to cardiovascular and renal alterations in adulthood. *Hypertension.* 2008;52(5):889-95.
25. Menon RT, Shrestha AK, Reynolds CL, Barrios R, and Shivanna B. Long-term pulmonary and cardiovascular morbidities of neonatal hyperoxia exposure in mice. *The international journal of biochemistry & cell biology.* 2018;94:119-24.
26. Patel JR, Barton GP, Braun RK, Goss KN, Haraldsdottir K, Hopp A, et al. Altered Right Ventricular Mechanical Properties Are Afterload Dependent in a Rodent Model of Bronchopulmonary Dysplasia. *Frontiers in physiology.* 2017;8:840.
27. Datta A, Kim GA, Taylor JM, Gugino SF, Farrow KN, Schumacker PT, et al. Mouse lung development and NOX1 induction during hyperoxia are developmentally regulated and mitochondrial ROS dependent. *American journal of physiology Lung cellular and molecular physiology.* 2015;309(4):L369-77.
28. Ramani M, Bradley WE, Dell'Italia LJ, and Ambalavanan N. Early exposure to hyperoxia or hypoxia adversely impacts cardiopulmonary development. *Am J Respir Cell Mol Biol.* 2015;52(5):594-602.
29. Yee M, Cohen ED, Domm W, Porter GA, Jr., McDavid AN, and O'Reilly MA. Neonatal hyperoxia depletes pulmonary vein cardiomyocytes in adult mice via mitochondrial oxidation. *American journal of physiology Lung cellular and molecular physiology.* 2018;314(5):L846-L59.
30. Mamchur S, Mamchur I, Khomenko E, Kokov A, Bokhan N, and Sherbinina D. Mechanical function of left atrium and pulmonary vein sleeves before and after their antrum isolation. *Medicina (Kaunas).* 2014;50(6):353-9.
31. Puente BN, Kimura W, Muralidhar SA, Moon J, Amatruda JF, Phelps KL, et al. The oxygen-rich postnatal environment induces cardiomyocyte cell-cycle arrest through DNA damage response. *Cell.* 2014;157(3):565-79.
32. Nagueh SF. Non-invasive assessment of left ventricular filling pressure. *Eur J Heart Fail.* 2018;20(1):38-48.
33. Mandinov L, Eberli FR, Seiler C, and Hess OM. Diastolic heart failure. *Cardiovasc Res.* 2000;45(4):813-25.
34. Gao S, Ho D, Vatner DE, and Vatner SF. Echocardiography in Mice. *Curr Protoc Mouse Biol.* 2011;1:71-83.
35. Scarpulla RC. Metabolic control of mitochondrial biogenesis through the PGC-1 family regulatory network. *Biochim Biophys Acta.* 2011;1813(7):1269-78.
36. Monteuuis G, Suomi F, Keratar JM, Masud AJ, and Kastaniotis AJ. A conserved mammalian mitochondrial isoform of acetyl-CoA carboxylase ACC1 provides the malonyl-CoA essential for mitochondrial biogenesis in tandem with ACSF3. *Biochem J.* 2017;474(22):3783-97.
37. Miklas JW, Clark E, Levy S, Detraux D, Leonard A, Beussman K, et al. TFPa/HADHA is required for fatty acid beta-oxidation and cardiolipin re-modeling in human cardiomyocytes. *Nat Commun.* 2019;10(1):4671.
38. Stein Y, and Stein O. Lipoprotein lipase and atherosclerosis. *Atherosclerosis.* 2003;170(1):1-9.

39. Tan M, Mosaoa R, Graham GT, Kasprzyk-Pawelec A, Gadre S, Parasido E, et al. Inhibition of the mitochondrial citrate carrier, Slc25a1, reverts steatosis, glucose intolerance, and inflammation in preclinical models of NAFLD/NASH. *Cell Death Differ.* 2020;27(7):2143-57.
40. Majd H, King MS, Smith AC, and Kunji ERS. Pathogenic mutations of the human mitochondrial citrate carrier SLC25A1 lead to impaired citrate export required for lipid, dolichol, ubiquinone and sterol synthesis. *Biochim Biophys Acta Bioenerg.* 2018;1859(1):1-7.
41. Chypre M, Zaidi N, and Smans K. ATP-citrate lyase: a mini-review. *Biochem Biophys Res Commun.* 2012;422(1):1-4.
42. Chen L, Duan Y, Wei H, Ning H, Bi C, Zhao Y, et al. Acetyl-CoA carboxylase (ACC) as a therapeutic target for metabolic syndrome and recent developments in ACC1/2 inhibitors. *Expert Opin Investig Drugs.* 2019;28(10):917-30.
43. Chirala SS, and Wakil SJ. Structure and function of animal fatty acid synthase. *Lipids.* 2004;39(11):1045-53.
44. Matsuzaka T, and Shimano H. Elovl6: a new player in fatty acid metabolism and insulin sensitivity. *J Mol Med (Berl).* 2009;87(4):379-84.
45. Dobrzyn P, Bednarski T, and Dobrzyn A. Metabolic reprogramming of the heart through stearoyl-CoA desaturase. *Prog Lipid Res.* 2015;57:1-12.
46. Rudolph MC, Wellberg EA, Lewis AS, Terrell KL, Merz AL, Maluf NK, et al. Thyroid hormone responsive protein Spot14 enhances catalysis of fatty acid synthase in lactating mammary epithelium. *J Lipid Res.* 2014;55(6):1052-65.
47. Li F, Gu Y, Dong W, Li H, Zhang L, Li N, et al. Cell death-inducing DFF45-like effector, a lipid droplet-associated protein, might be involved in the differentiation of human adipocytes. *FEBS J.* 2010;277(20):4173-83.
48. den Ruijter HM, Pasterkamp G, and de Jager SC. Adiponectin regulation in cardiovascular disease: is diseased fat showing its true color? *Arterioscler Thromb Vasc Biol.* 2014;34(10):2180-1.
49. Rossato FA, Zecchin KG, La Guardia PG, Ortega RM, Alberici LC, Costa RA, et al. Fatty acid synthase inhibitors induce apoptosis in non-tumorigenic melan-a cells associated with inhibition of mitochondrial respiration. *PloS one.* 2014;9(6):e101060.
50. Carvalho MA, Zecchin KG, Seguin F, Bastos DC, Agostini M, Rangel AL, et al. Fatty acid synthase inhibition with Orlistat promotes apoptosis and reduces cell growth and lymph node metastasis in a mouse melanoma model. *Int J Cancer.* 2008;123(11):2557-65.
51. Wang G, Li Z, Li X, Zhang C, and Peng L. RASAL1 induces to downregulate the SCD1, leading to suppression of cell proliferation in colon cancer via LXRalpha/SREBP1c pathway. *Biol Res.* 2019;52(1):60.
52. Igal RA. Stearoyl-CoA desaturase-1: a novel key player in the mechanisms of cell proliferation, programmed cell death and transformation to cancer. *Carcinogenesis.* 2010;31(9):1509-15.
53. Igal RA. Roles of StearoylCoA Desaturase-1 in the Regulation of Cancer Cell Growth, Survival and Tumorigenesis. *Cancers (Basel).* 2011;3(2):2462-77.
54. Claycomb WC, Lanson NA, Jr., Stallworth BS, Egeland DB, Delcarpio JB, Bahinski A, et al. HL-1 cells: a cardiac muscle cell line that contracts and retains phenotypic characteristics of the adult cardiomyocyte. *Proceedings of the National Academy of Sciences of the United States of America.* 1998;95(6):2979-84.
55. Xu HF, Luo J, Zhao WS, Yang YC, Tian HB, Shi HB, et al. Overexpression of SREBP1 (sterol regulatory element binding protein 1) promotes de novo fatty acid synthesis and triacylglycerol accumulation in goat mammary epithelial cells. *J Dairy Sci.* 2016;99(1):783-95.
56. Tracz-Gaszewska Z, and Dobrzyn P. Stearoyl-CoA Desaturase 1 as a Therapeutic Target for the Treatment of Cancer. *Cancers (Basel).* 2019;11(7).
57. Falvella FS, Pascale RM, Gariboldi M, Manenti G, De Miglio MR, Simile MM, et al. Stearoyl-CoA desaturase 1 (Scd1) gene overexpression is associated with genetic predisposition to hepatocarcinogenesis in mice and rats. *Carcinogenesis.* 2002;23(11):1933-6.
58. Flavin R, Peluso S, Nguyen PL, and Loda M. Fatty acid synthase as a potential therapeutic target in cancer. *Future Oncol.* 2010;6(4):551-62.

59. Lu T, Sun L, Wang Z, Zhang Y, He Z, and Xu C. Fatty acid synthase enhances colorectal cancer cell proliferation and metastasis via regulating AMPK/mTOR pathway. *Onco Targets Ther.* 2019;12:3339-47.
60. Scaglia N, and Igal RA. Stearoyl-CoA desaturase is involved in the control of proliferation, anchorage-independent growth, and survival in human transformed cells. *J Biol Chem.* 2005;280(27):25339-49.
61. Eimre M, Paju K, Pelloux S, Beraud N, Roosimaa M, Kadaja L, et al. Distinct organization of energy metabolism in HL-1 cardiac cell line and cardiomyocytes. *Biochim Biophys Acta.* 2008;1777(6):514-24.
62. Kuznetsov AV, Javadov S, Sickinger S, Frotschnig S, and Grimm M. H9c2 and HL-1 cells demonstrate distinct features of energy metabolism, mitochondrial function and sensitivity to hypoxia-reoxygenation. *Biochim Biophys Acta.* 2015;1853(2):276-84.
63. Menendez JA, and Lupu R. Fatty acid synthase and the lipogenic phenotype in cancer pathogenesis. *Nat Rev Cancer.* 2007;7(10):763-77.
64. Wang Q, Du X, Zhou B, Li J, Lu W, Chen Q, et al. Mitochondrial dysfunction is responsible for fatty acid synthase inhibition-induced apoptosis in breast cancer cells by PdpaMn. *Biomed Pharmacother.* 2017;96:396-403.
65. Matsui H, Yokoyama T, Sekiguchi K, Iijima D, Sunaga H, Maniwa M, et al. Stearoyl-CoA desaturase-1 (SCD1) augments saturated fatty acid-induced lipid accumulation and inhibits apoptosis in cardiac myocytes. *PloS one.* 2012;7(3):e33283.
66. Chen L, Ren J, Yang L, Li Y, Fu J, Li Y, et al. Stearoyl-CoA desaturase-1 mediated cell apoptosis in colorectal cancer by promoting ceramide synthesis. *Sci Rep.* 2016;6:19665.
67. Dobrzyn P, Dobrzyn A, Miyazaki M, Cohen P, Asilmaz E, Hardie DG, et al. Stearoyl-CoA desaturase 1 deficiency increases fatty acid oxidation by activating AMP-activated protein kinase in liver. *Proceedings of the National Academy of Sciences of the United States of America.* 2004;101(17):6409-14.
68. Dobrzyn P, Sampath H, Dobrzyn A, Miyazaki M, and Ntambi JM. Loss of stearoyl-CoA desaturase 1 inhibits fatty acid oxidation and increases glucose utilization in the heart. *Am J Physiol Endocrinol Metab.* 2008;294(2):E357-64.
69. Shaw RJ. LKB1 and AMP-activated protein kinase control of mTOR signalling and growth. *Acta Physiol (Oxf).* 2009;196(1):65-80.
70. Li Y, Xu S, Mihaylova MM, Zheng B, Hou X, Jiang B, et al. AMPK phosphorylates and inhibits SREBP activity to attenuate hepatic steatosis and atherosclerosis in diet-induced insulin-resistant mice. *Cell Metab.* 2011;13(4):376-88.
71. Meyburg J, Schulze A, Kohlmueller D, Poschl J, Linderkamp O, Hoffmann GF, et al. Acylcarnitine profiles of preterm infants over the first four weeks of life. *Pediatr Res.* 2002;52(5):720-3.
72. Wende AR, Brahma MK, McGinnis GR, and Young ME. Metabolic Origins of Heart Failure. *JACC Basic Transl Sci.* 2017;2(3):297-310.
73. Staels B, and Fruchart JC. Therapeutic roles of peroxisome proliferator-activated receptor agonists. *Diabetes.* 2005;54(8):2460-70.
74. Xu HF, Luo J, Zhang XY, Li J, and Bionaz M. Activation of liver X receptor promotes fatty acid synthesis in goat mammary epithelial cells via modulation of SREBP1 expression. *J Dairy Sci.* 2019;102(4):3544-55.
75. Repa JJ, Liang G, Ou J, Bashmakov Y, Lobaccaro JM, Shimomura I, et al. Regulation of mouse sterol regulatory element-binding protein-1c gene (SREBP-1c) by oxysterol receptors, LXRalpha and LXRbeta. *Genes Dev.* 2000;14(22):2819-30.
76. Wang B, and Tontonoz P. Liver X receptors in lipid signalling and membrane homeostasis. *Nat Rev Endocrinol.* 2018;14(8):452-63.
77. Kadegowda AK, Bionaz M, Piperova LS, Erdman RA, and Loor JJ. Peroxisome proliferator-activated receptor-gamma activation and long-chain fatty acids alter lipogenic gene networks in bovine mammary epithelial cells to various extents. *J Dairy Sci.* 2009;92(9):4276-89.

78. Carvalho BS, and Irizarry RA. A framework for oligonucleotide microarray preprocessing. *Bioinformatics.* 2010;26(19):2363-7.
79. Ritchie ME, Phipson B, Wu D, Hu Y, Law CW, Shi W, et al. limma powers differential expression analyses for RNA-sequencing and microarray studies. *Nucleic acids research.* 2015;43(7):e47.
80. Yee M, Vitiello PF, Roper JM, Staversky RJ, Wright TW, McGrath-Morrow SA, et al. Type II epithelial cells are critical target for hyperoxia-mediated impairment of postnatal lung development. *American journal of physiology Lung cellular and molecular physiology.* 2006;291(5):L1101-11.
81. Bandyopadhyay G, Huyck HL, Misra RS, Bhattacharya S, Wang Q, Mereness J, et al. Dissociation, cellular isolation, and initial molecular characterization of neonatal and pediatric human lung tissues. *American journal of physiology Lung cellular and molecular physiology.* 2018;315(4):L576-L83.
82. Ardini-Poleske ME, Clark RF, Ansong C, Carson JP, Corley RA, Deutsch GH, et al. LungMAP: The Molecular Atlas of Lung Development Program. *American journal of physiology Lung cellular and molecular physiology.* 2017;313(5):L733-L40.

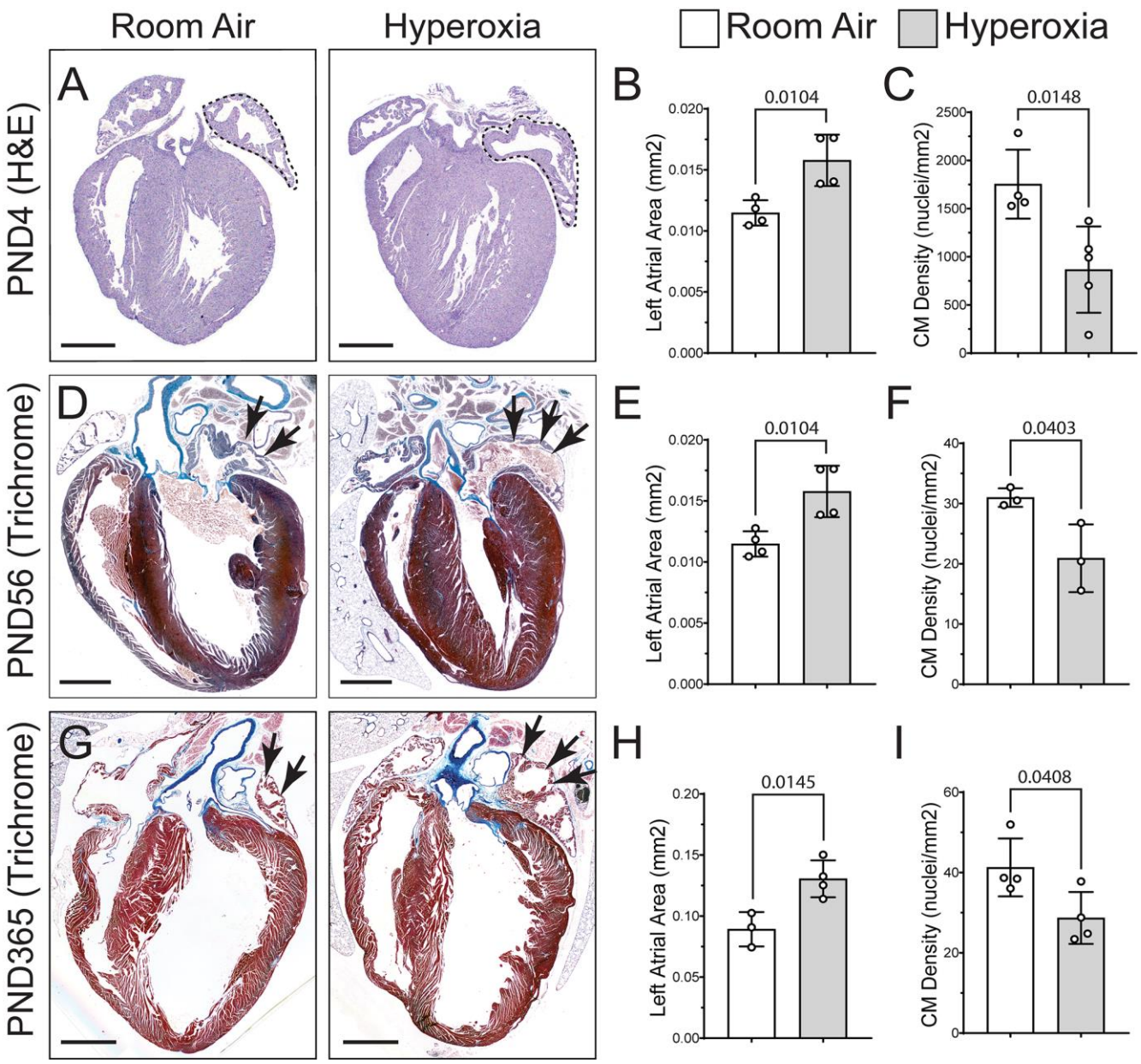


Figure 1. Neonatal hyperoxia enlarges the left atria of mice but reduces the density of cardiomyocyte (CM) nuclei in the left atrial myocardia. (A) Hematoxylin and eosin (H&E) stained sections of hearts from postnatal day (PND) 4 mice that were exposed to room air (left) or hyperoxia (right). Dotted lines outline the left atria. (B) Mean area of the left atria in sections of room air and hyperoxia exposed mice on PND4. N=4 mice per condition. (C) Numbers of DAPI stained nuclei per $mm^2$ of TNNT2+ myocardium. Room air n=4; hyperoxia n=5 mice per condition. (D, G) Sectioned hearts of PND56 (D) and PND365 (G) mice exposed to room air (right) or hyperoxia (right) from PND0-4 stained with Masson's trichrome. (E, H) Graphs show mean area of the left atria in sections of room air and hyperoxia-exposed mice on PND56 (E) and PND365 (F). (E) N=4 per condition. (H) Room air n=3; hyperoxia n=4. (F, I) Graphs show numbers of DAPI stained nuclei per mm2 of TNNT2+ myocardium in room air and hyperoxia-exposed mice on PND56 (F) and PND365 (I). (F) N=3 mice per condition. (I) N=4 mice per condition. Box plots show median, second and third quartiles, whiskers indicate the range and circles show individual data points. The p-values between datasets are from unpaired t-tests.

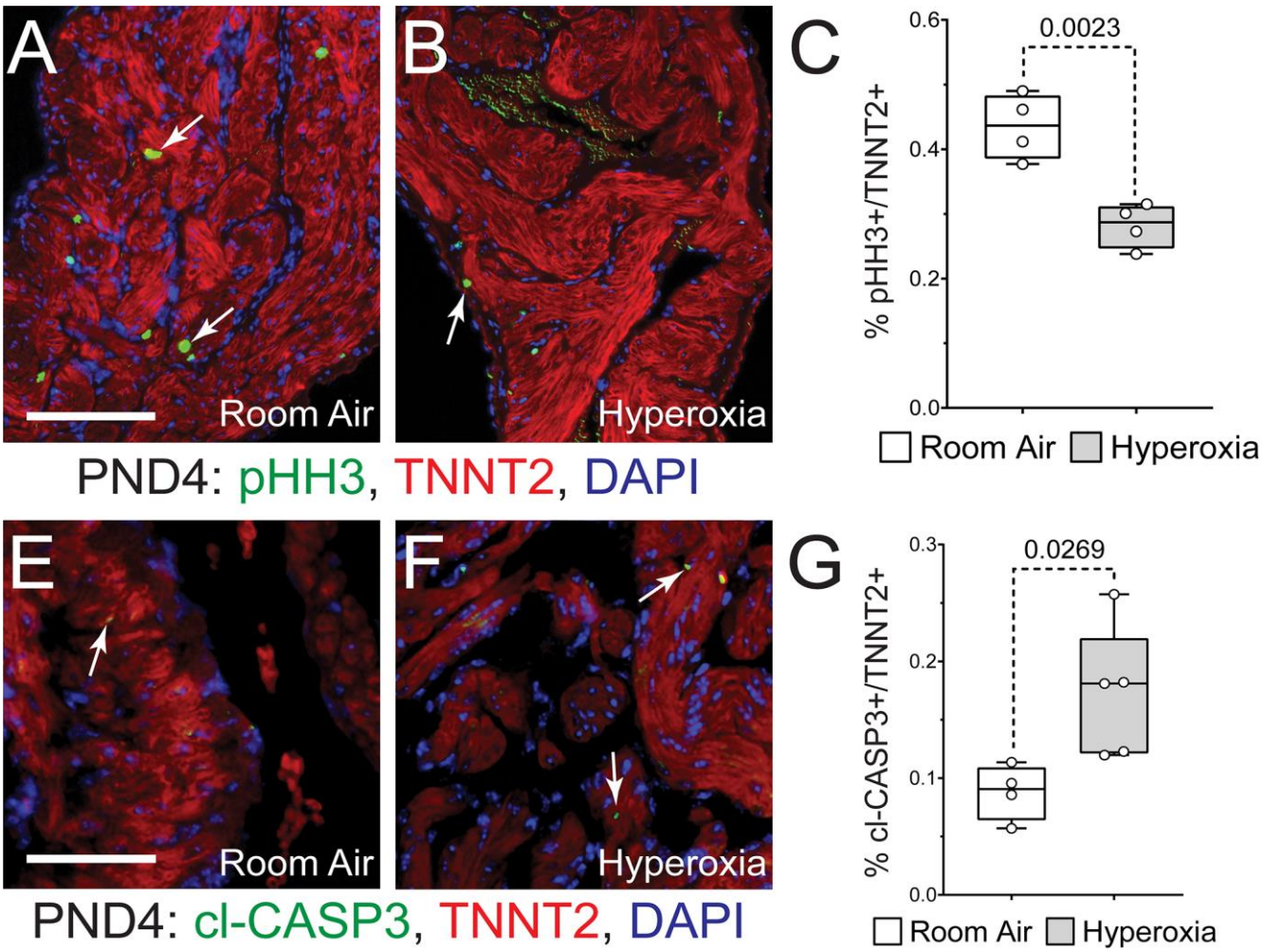


Figure 2. Hyperoxia reduces postnatal proliferation and survival of left atrial cardiomyocytes in neonatal mice. (A, B) Sections of left atrial appendages from PND4 control (A) and hyperoxia-exposed (B) mice stained with phosphorylated Histone H3 (pHH3, green), cardiac troponin T (TNNT2, red) and 4′,6-diamidino-2-phenylindole (DAPI, blue). Arrows point to pHH3+ cardiomyocytes. (C) Percentage of pHH3+ cardiomyocytes in PND4 mice exposed to room air or hyperoxia. N=4 mice per condition. (E, F) Sectioned left atrial appendages of PND4 control (E) and hyperoxia-exposed (F) mice stained for the active, cleaved form of Caspase 3 (cl-Casp3), TNNT2 and DAPI. Arrows point to cl-Casp3+ cardiomyocytes. (G) Percentage of cl-Casp3 labeled CMs in the left atria of PND4 hyperoxia-exposed and control mice. Room air n=4, hyperoxia n=5 mice per condition. Box plots show median, second and third quartiles, whiskers indicate range and circles represent individual data points. P-values are results of unpaired t-tests. (A, E) Scale bars = 200 μm.

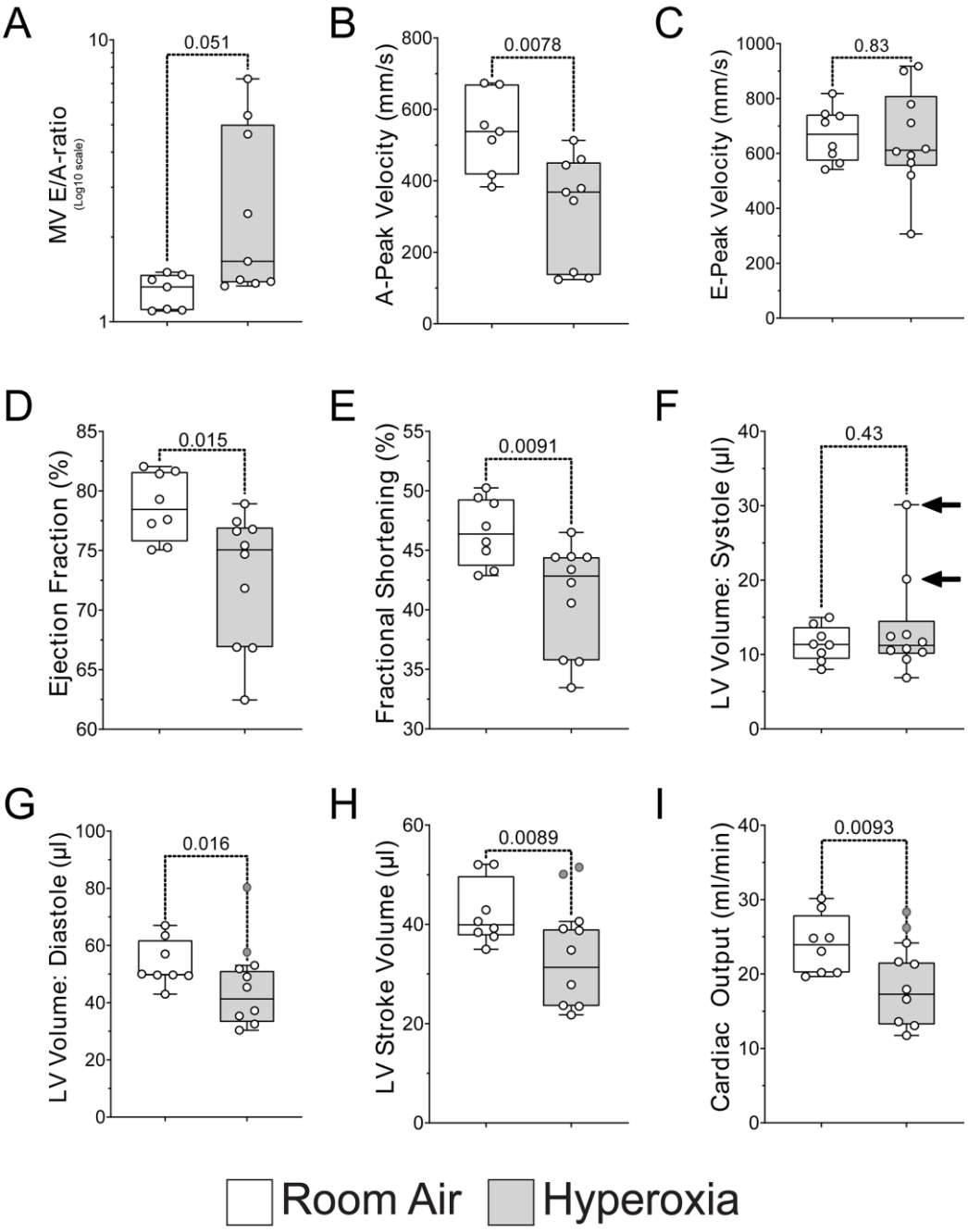


Figure 3. Neonatal hyperoxia causes mice to develop dilated heart failure later in life. (A, B, C) Graphs show mean E/A ratios (A), A-peak velocities (B) and E-peak velocities (C) of blood flow across the mitral valves of control and hyperoxia-exposed mice on PND365. E/A ratios are plotted on a log10 scale. (D, E) Graphs show mean ejection fraction (D) and fractional shortening (E) of control and hyperoxia-exposed mice on PND365. (F) Graph shows mean volume of the left ventricle during systole for PNDD365 control and hyperoxia-exposed mice. Arrows point to two hyperoxia-exposed mice with left ventricles that were drastically enlarged relative to controls and other hyperoxia-exposed mice. These two mice had the highest E/A ratios of all mice. (G-I) Box plots show the mean diastolic volume (G), stroke volume (H) and cardiac output (I) of the left ventricles in PND365 hyperoxia-exposed and control mice after the two mice with enlarged left ventricular systolic volumes were excluded. Grey circles are values for excluded mice. Box plots show median, second and third quartiles, whiskers show range and circles show individual data points. F-tests were used to determine if values for control and hyperoxia-exposed mice had equal variances. The p-values are from unpaired t-tests.

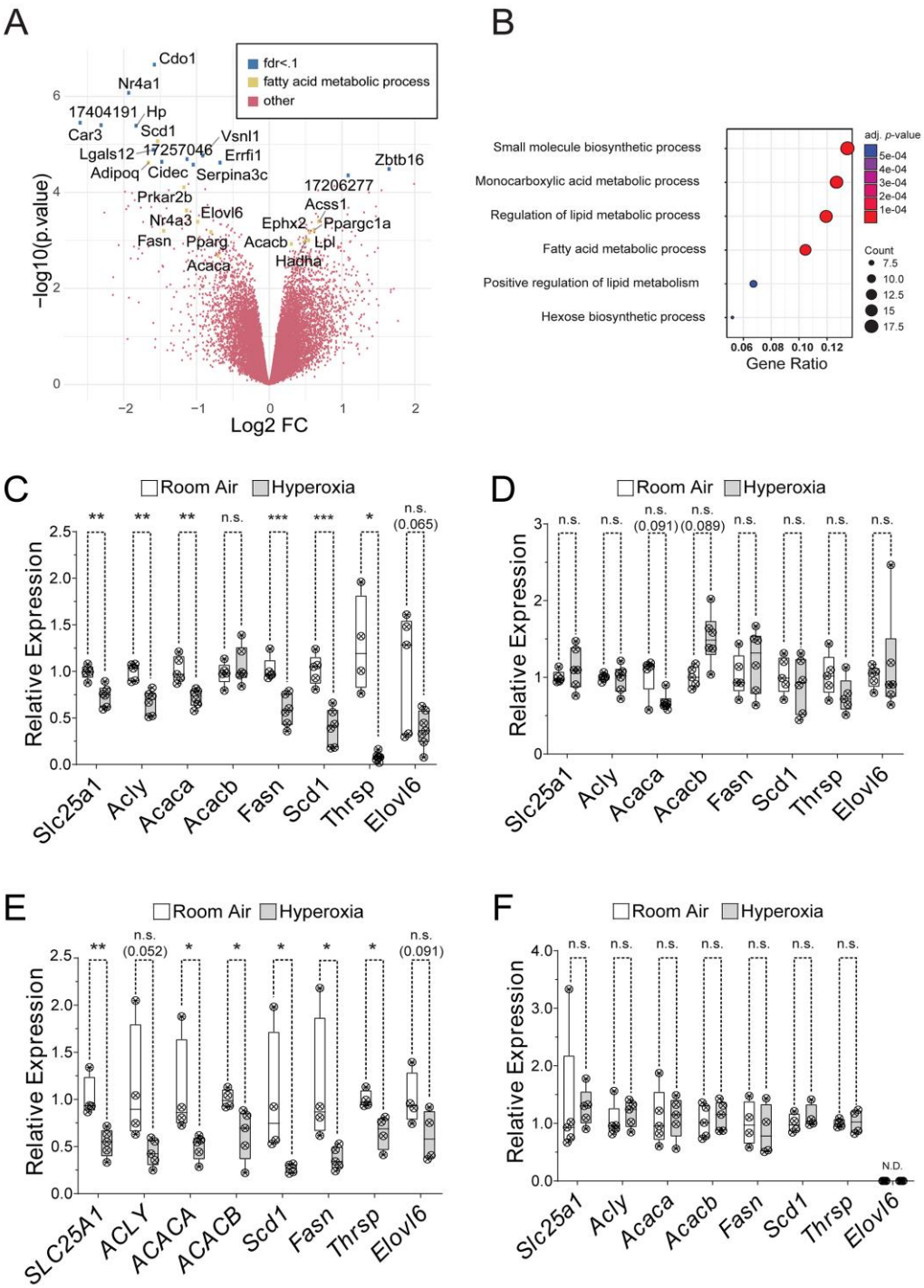


Figure 4. Neonatal hyperoxia suppresses genes needed for fatty acid synthesis in atria of mice. (A) Volcano plot of Log2 fold changes vs log10 p-values. Genes with FDR < 10% or annotation in the fatty acid metabolism are highlighted. Genes with false discovery rate <0.1 are marked by blue dots, genes involved in fatty acid metabolism are marked by green dots. (B) Gene ontology (GO) analysis of differentially expressed genes. (C-F) Results of qRT-PCR for *Slc25a1, Acly, Acaca, Acacb*, *Fasn*, *Scd1*, *Thrsp* and *Elovl6* in atria (C, E) and ventricles (D, E) of hyperoxia-exposed and control mice on PND4 (C, D) and PND56 (E, F). (A, B) room air n=3; hyperoxia n=4, (C-E) room air n=5; hyperoxia n=6, (F) *Slc25a1, Acly, Acaca, AcacB*, room air n=5; hyperoxia n=5, *Scd1, Fasn, Thrsp, Elovl6*, room air n=4; hyperoxia n=4. (C-F) Box plots show median and inner quartiles. Error bars show range. Circles show values for individual control and hyperoxia-exposed mice, respectively. (C-F) Asterisks indicate significance with p-values * < 0.05, ** <0.01, *** < 0.005, **** <0.001 using unpaired t-tests.

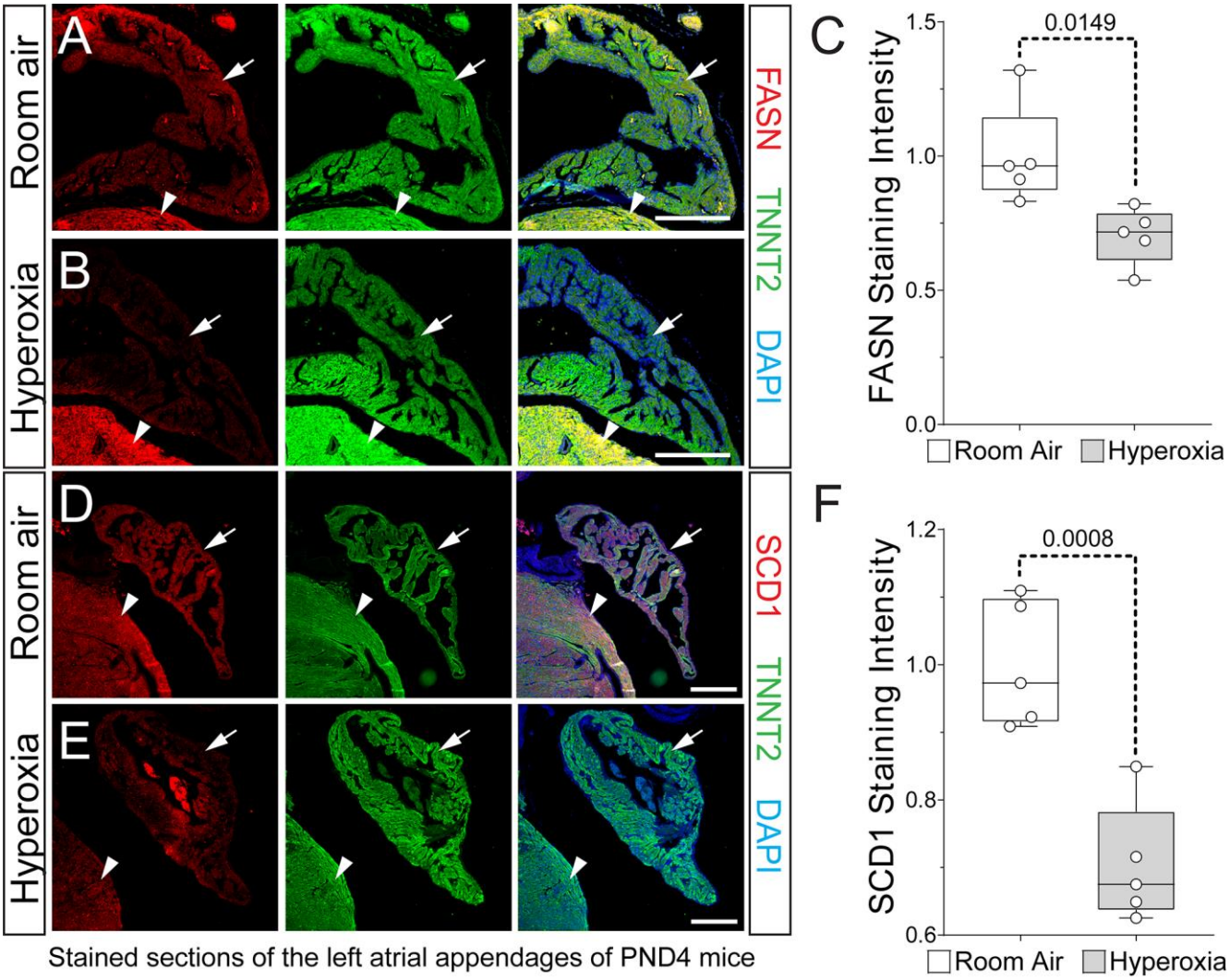


Figure 5. Neonatal hyperoxia represses fatty acid synthesis enzymes in murine atrial cardiomyocytes. (A, B, D, E). Sections of left atrial appendages from PND4 neonates exposed to room air (A, B) or hyperoxia (D, E) co-stained for FASN (red, A and B) or SCD1 (red, D and E) and TNNT2 (green, A, B, D, E). Sections were also stained with DAPI to label nuclei (blue, A, B, D, E). Arrows and arrowheads show TNNT2+ cardiomyocytes in left atrial appendage and LV, respectively. Scale bars = 200 μm. (C, F) Graphs show relative staining intensities for *Fasn* (C) and *Scd1* (F) measured using NIH ImageJ 2.0/Fiji. (C, F) Numbers: room air n=5; hyperoxia n=5. Box plots show median values and inner quartiles. Error bars show the range of values. Circles show values for individual room air and hyperoxia-exposed mice, respectively. F-tests were used to determine if samples had equal or unequal variances. P-values are the results of unpaired t-tests. Scale bars = 400 μm (A) or 1000 μm (D, G).

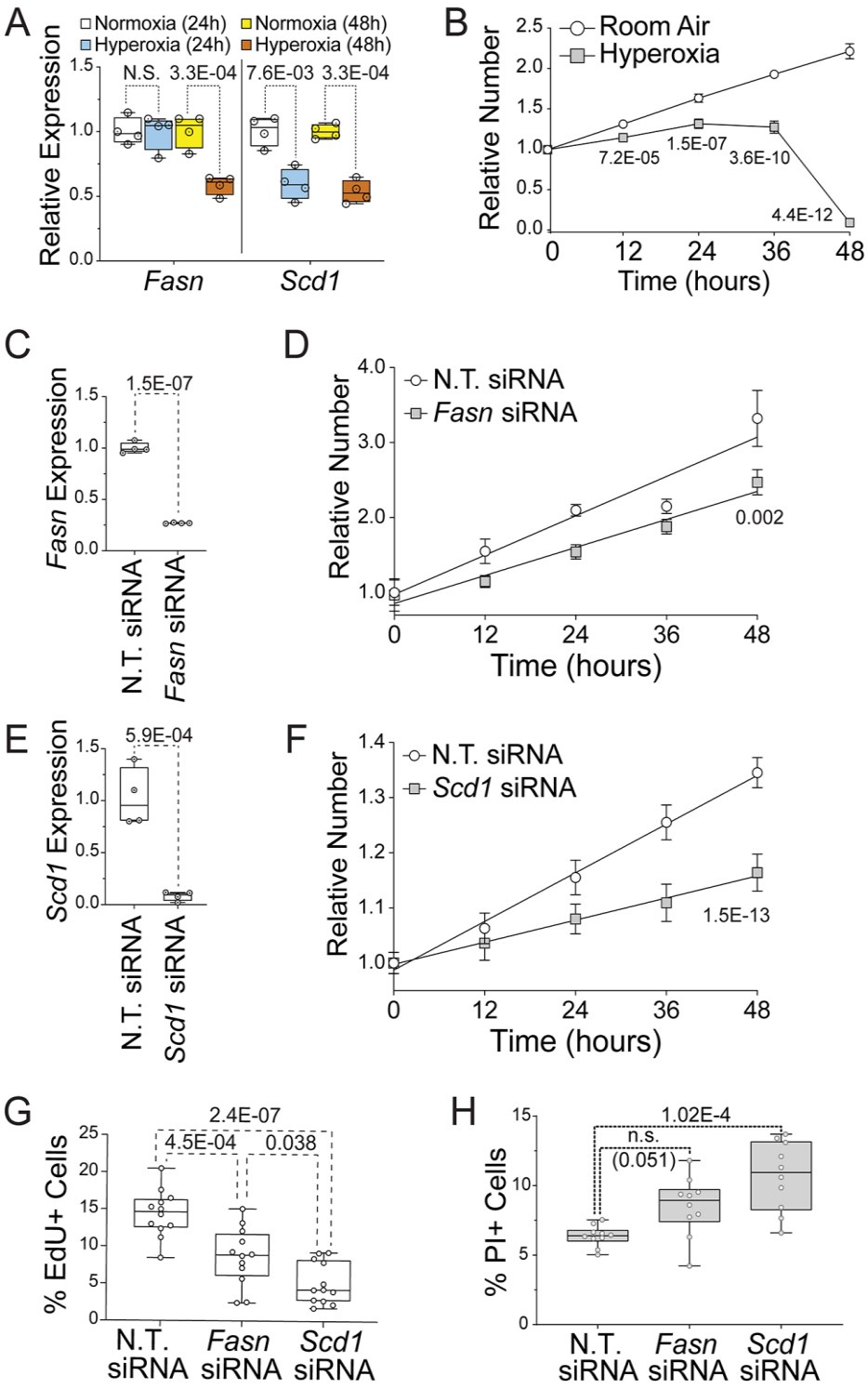


Figure 6. Suppression of fatty acid synthesis contributes to reduced HL-1 cell proliferation in hyperoxia. (A) qRT-PCR for *Fasn* (left) and *Scd1* (right) in HL-1 cells grown in room air or hyperoxia for 24 hours (white and blue, respectively) or 48 hours (yellow and red, respectively). (B) Numbers of HL-1 cells grown in room air (white circles) and hyperoxia (gray squares) for 48 hours relative to their density at 0 hours. (C and D) qRT-PCR for *Fasn* (C) and *Scd1* (E) in HL-1 cells transfected with *Fasn* and *Scd1* siRNAs. Controls were transfected with non-targeting (N.T.) siRNA. (D and F) Numbers of HL-1 cells transfected with control siRNA (white circles in D and F) and *Fasn* (Gray squares in D) or *Scd1* (Gray squares in F) siRNAs and grown for 48 hours in room air relative to 0 hrs. (G) HL-1 cells transfected with N.T., *Fasn* and *Scd1* siRNAs, grown in room air for 22 hours and treated with EdU for 2 hours before staining. Graph shows percentages of EdU+ cells. (H) HL-1 cells transfected with N.T., *Fasn* and *Scd1* siRNAs were grown in room air for 48 hours, stained with PI and imaged. Graph shows numbers of PI+ N.T., *Fasn* and *Scd1* siRNA transfected cells. (A, C, E) N=5 transfections per condition. Numbers: (B, D, F) Each time/condition n=24 (G) n=12 and (H) n=10. (B, D, and F) Error bars show 95% CI, lines and p-values are results of linear regressions (A, C, E, G and H) Box plots are median, 2nd and 3rd quartiles, error bars indicate range and markers show individual replicates. P-values are from unpaired t-tests (C and E) or one-way ANOVA with Holm-Sidak corrections (A, G and H).

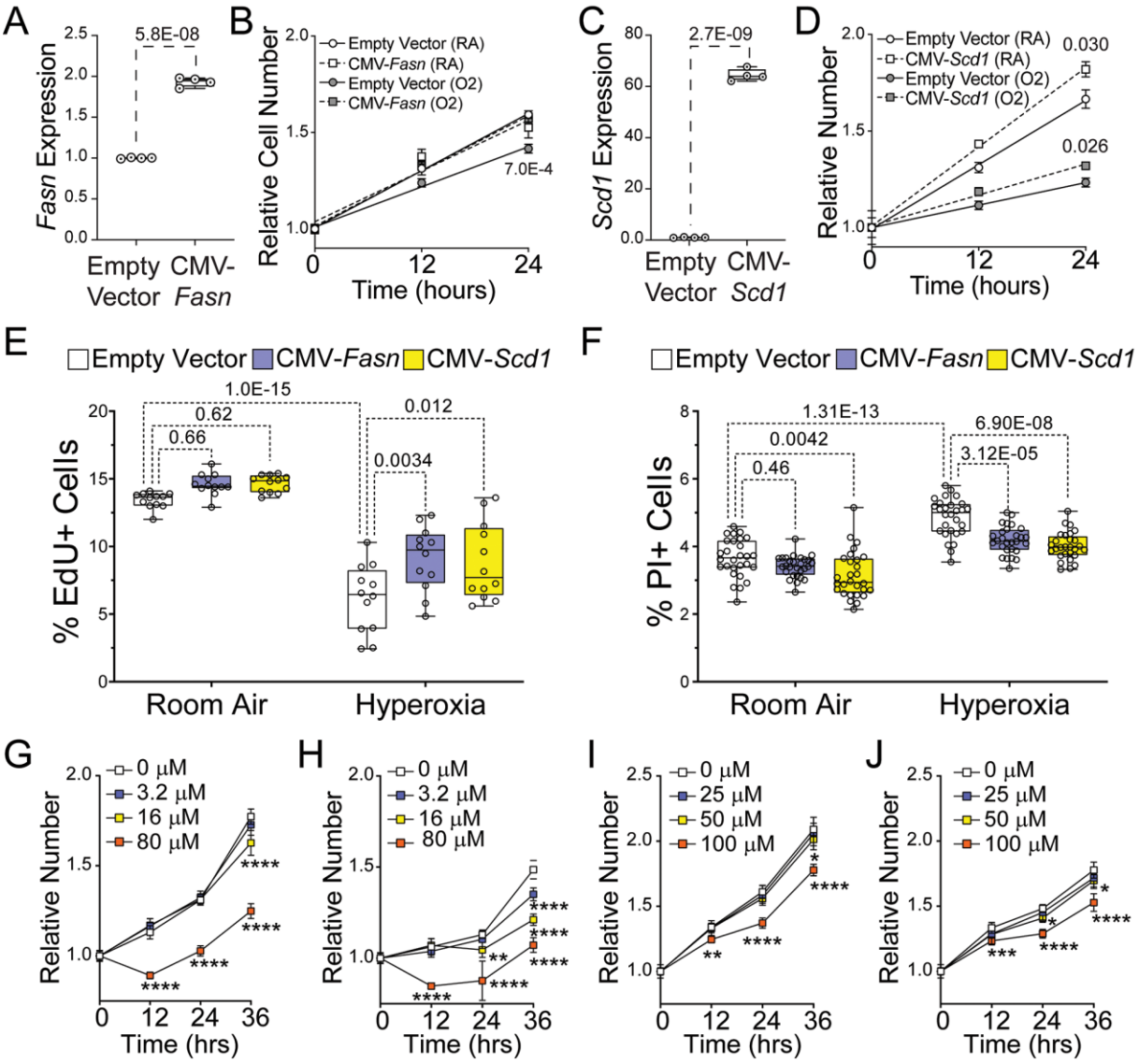


Figure 7. *Fasn* and *Scd1* overexpression increases HL-1 cell proliferation in hyperoxia. (A and C) *Fasn* (A) and *Scd1* (C) mRNA in HL-1 cells 48 hours after transfection with empty vector or *Fasn* (A) and *Scd1* (C) expression vectors. N=4 transfections per condition. (B and D) Expansion of *Fasn* (B), *Scd1* (D) and control transfected HL-1 cells over 24 hours. Markers are mean fold change in cell number for control (circles), *Fasn* (squares with dashed line, B) and *Scd1* (squares with dashed line, D) grown in room air (white) or hyperoxia (gray). Lines and p-values are linear regressions. N=10 wells per time/condition. (E) Percentages of EdU+ control (white), *Fasn* (blue) and *Scd1* (yellow) transfected HL-1 cells after 2 hours incubation in room air (left), and hyperoxia (right). N=12 wells per condition. (F) Percentages of control (white), *Fasn* (blue) and *Scd1* (yellow) transfected cells labeled after PI staining in room (left) and hyperoxia (right). N=28 wells per condition. (G, H) HL-1 cell expansion in media with 0, 3.2, 16 and 80μM palmitate-BSA in room air (G) or hyperoxia (H) for 36 hours. (I, J) Expansion of HL-1 cells in media containing 0, 25, 50 and 100mM oleate-BSA and grown in room air (I) or hyperoxia (J) for 36 hours. (A, C, E and F) Box plots show median, second and third quartiles, markers represent individual values, error bars show range. P-values are results of unpaired t-tests (A and C) or one-way ANOVA with Holmes-Sidak corrections. (B, D) Trendlines and p-values linear regressions. (G, H, I and J) N=18 wells per time/condition. Asterisks indicate significance with p-values * < 0.05, ** <0.01, *** < 0.005, **** <0.001 using two-way ANOVA with Tukey's multiple comparison tests.

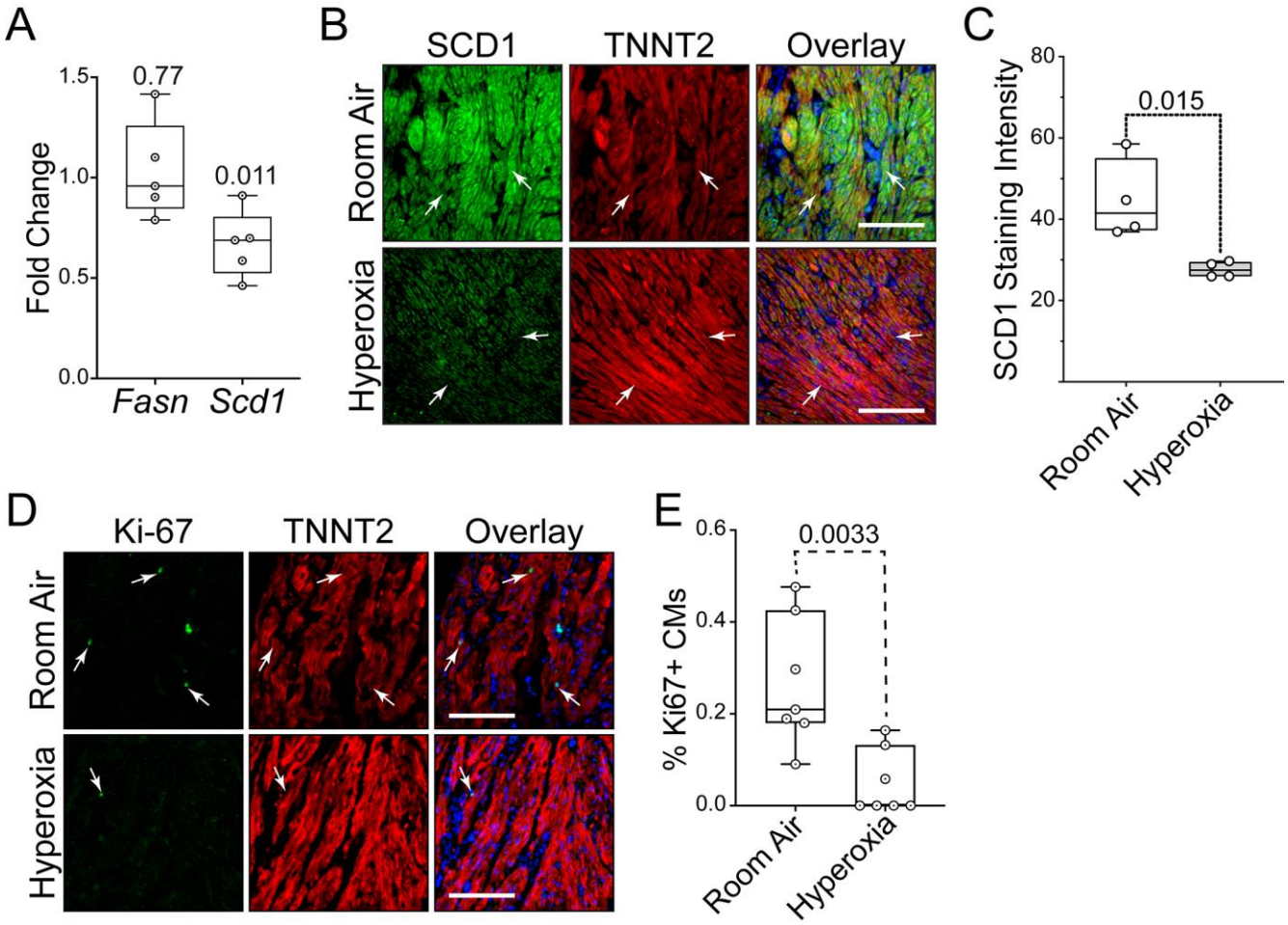


Figure 8. Hyperoxia suppresses fatty acid synthesis genes in left atrial tissue explanted from human infants. (A) Results of qRT-PCR for *Fasn* and *Scd1* in left atrial tissue explanted from human infants who died at birth due to anencephaly and exposed to room air or hyperoxia for 24 hours. N=5 donors. (B) Sectioned explants exposed to room air (top) or hyperoxia (bottom) were stained for SCD1 (green), TNNT2 (red) and DAPI (blue). (C) Graph shows staining intensities for SCD1 in sections of control and hyperoxia-exposed mice determined using NIH ImageJ 2.0/Fiji. N=4 donors. (D) Sections of explants exposed to room air (top) and hyperoxia (bottom) stained for the proliferation marker Ki67 (green), TNNT2 (red) and DAPI (blue). (E) Graph shows percentages of TNNT2 expressing cells with Ki67+ nuclei in explants exposed to room air or hyperoxia. N=7 donors. (A, C and E) Circles indicate individual values for explants of each donor. Boxes show medians and inner quartiles, error bars represent the range and p-values are the results of either single sample t and Wilcox tests (A) or unpaired t-tests (C and E). (B, D) Scale bars = 100 μm.